Accepted Manuscript

Journal of the Geological Society

The Neoarchaean Uyea Gneiss Complex, Shetland: an onshore fragment of the Rae Craton on the European Plate

P.D. Kinny, R.A. Strachan, M. Fowler, C. Clark, S. Davis, I. Jahn, R.J.M. Taylor, R.E. Holdsworth & E. Dempsey

DOI: https://doi.org/10.1144/jgs2019-017

Received 7 February 2019
Revised 11 May 2019
Accepted 14 May 2019

The Neoarchaean Uyea Gneiss Complex, Shetland: an onshore fragment of the Rae Craton on the European Plate

P.D. Kinny[1], R.A. Strachan[2], M. Fowler[2], C. Clark[1], S. Davis[1,3], I. Jahn[1,4], R.J.M. Taylor[1,5], R.E. Holdsworth[6] & E. Dempsey[7]

1. The Institute for Geoscience Research (TIGeR), School of Earth and Planetary Sciences, Curtin University, Perth, WA 6845, Australia

2. School of Earth & Environmental Sciences, University of Portsmouth, Portsmouth, PO1 3QL, UK

3. Present Address: shaunpauldavis@gmail.com

4. Present address: inalee.jahn@postgrad.curtin.edu.au

5. Present Address: Department of Earth Sciences, University of Cambridge, CB2 3EQ, UK

6. Department of Earth Sciences, Durham University, Durham, DH1 3LE, UK

7. School of Environmental Sciences, University of Hull, Hull, HU6 7RX, UK

Abstract:

A tract of amphibolite facies granitic gneisses and metagabbros in northern Shetland, U.K., is here named the Uyea Gneiss Complex. Zircon U–Pb dating indicates emplacement of the igneous protoliths of the complex *c.* 2746–2726 Ma, at a later time than most of the Archaean protoliths of the Lewisian Gneiss Complex of mainland Scotland. Calc-alkaline geochemistry of the Uyea Gneiss Complex indicates arc-affinity and a strong genetic kinship among the mafic and felsic components. Zircon Hf compositions suggest an enriched mantle source and limited interaction with older crust during emplacement. Ductile fabrics developed soon after emplacement, with zircon rims at *c.* 2710 Ma, but there was little further deformation until Caledonian reworking east of the Uyea Shear Zone. There is no evidence for the Palaeoproterozoic reworking that dominates large tracts of the Lewisian Gneiss Complex and of the Nagssugtoqidian Orogen of East Greenland. The more northerly location of the Uyea Gneiss Complex and extensive offshore basement of similar age implies that, prior to the opening of the North Atlantic Ocean, these rocks were contiguous with the Archaean Rae Craton.

End of abstract

In northern Scotland, the Archaean–Palaeoproterozoic Lewisian Gneiss Complex forms the basement of the foreland of the Ordovician–Silurian Caledonide Orogen. There, the western limit of the orogen is defined by the easterly-dipping Moine Thrust (Fig. 1). Within the Caledonian hinterland east of the Moine Thrust, metasediments of the Moine Supergroup occur in a series of thrust sheets, together with a number of Neoarchaean basement inliers. Where dated, these inliers have recorded ages matching parts of the foreland Lewisian Gneiss Complex (Friend et al. 2008). Overall, the Lewisian Gneiss Complex represents an assemblage of fragments of the Laurentian palaeocontinent that was detached and transferred to the European Plate during the Mesozoic–Tertiary rifting that formed the North Atlantic Ocean. The Complex is dominated by Archaean TTG-suite orthogneisses, the protoliths of which were emplaced between *c.* 3.1 – 2.7 Ga, subjected to high-grade metamorphism *c.* 2.7 – 2.5 Ga, intruded by mafic dykes *c.* 2.4 Ga and variably reworked and intruded by granites *c.* 1.8 – 1.7 Ga (e.g. Whitehouse 1993; Kinny & Friend 1997; Friend & Kinny 2001; Whitehouse & Bridgwater 2001; Kinny et al. 2005; Park 2005; Wheeler et al. 2010; Mason 2012; Goodenough et al. 2013; Davies & Heaman 2014; Crowley et al. 2015). This geological history is very similar to that of the Nagssugtoqidian Orogen of southern Greenland, and the two segments of crust are thought to have been contiguous prior to opening of the North Atlantic Ocean (Friend & Kinny 2001; Park 2005).

Situated some two hundred kilometres north of the Scottish coastline, the Shetland island group provides the northernmost exposures of the Caledonide Orogen in the British Isles (Fig. 1). Much of Shetland is underlain by Neoproterozoic to Cambrian metasedimentary successions which, like the Moine Supergroup on mainland Scotland, were deformed and metamorphosed during the Caledonian orogeny (Flinn 1985; 1988). At the northern tip of the main island of the Shetland group, the easterly-dipping Wester Keolka Shear Zone is thought to be structurally analogous to the Moine Thrust (Fig. 1; Pringle 1970; Flinn 1985, *cf.* Walker *et al.* 2016), and in its footwall, a series of variably reworked granitic gneisses and metagabbros is exposed. On the basis of structural position, lithological similarities and K–Ar geochronology (Pringle 1970; Flinn et al. 1979; Flinn 1985, 2009), this orthogneiss complex has been correlated with the Lewisian. In this paper we investigate the geochemistry and age relationships of these well-preserved, ancient orthogneisses on Shetland in greater detail, and compare them to the Lewisian gneisses.

Geological setting and field relationships

The meta-igneous rocks of northwest Shetland were described by Pringle (1970) and Flinn (2009) who defined the Uyea and Wilgi Geos 'groups' as those exposed, respectively, west and east of the easterly-dipping Uyea Shear Zone (Figs 1 and 2). The two 'groups' appear to have similar meta-igneous protoliths and differ only in the significantly greater degree of ductile deformation that has been superimposed on the Wilgi Geos group. Because the protoliths are in all cases thought to have been intrusive igneous rocks, it is no longer useful to refer to these units as 'groups' *sensu* Pringle (1970). Instead, we propose the term 'Uyea Gneiss Complex' to refer to all the meta-igneous rocks in the footwall of Wester Keolka Shear Zone.

The Uyea Gneiss Complex in the footwall of the Uyea Shear Zone.

This segment of the complex (Fig. 2) is very well exposed along the coast, but inland exposures are scarce. It is the least deformed part of the complex and has yielded K–Ar and $^{40}Ar/^{39}Ar$ biotite and amphibole ages of *c.* 2440–2900 Ma (Flinn *et al.* 1979; Robinson 1983). It comprises two main lithologies: granitic gneiss and metagabbro. There are three metagabbro bodies: the major Fugla Ness body and smaller Blue Head and North Wick intrusions (Fig. 2). The weakly deformed granitoid exposed on the island of Uyea (Fig. 2) appears to be a less deformed equivalent of the granitic gneiss but it has not been examined during the current study.

Granitic gneiss.

The coastal section is dominated by medium- to coarse-grained granitic gneiss. This carries a heterogeneously-developed foliation which is moderately to steeply N–NW-dipping and trends E–NE (Fig. 2). Finite strains are generally low to moderate. The foliation is typically defined by trails of mica (biotite and muscovite) and grains of recrystallized quartz, often wrapping lenticular augen of plagioclase and/or K-feldspar (Fig. 3a). Evidence for high-temperature (>500˚C) deformation is provided by the myrmekite fringes to feldspar augen. In places, cm-scale mineralogical variations define a banded, gneissic fabric. However, there is no evidence that the granitic gneiss has ever undergone high-temperature segregation or migmatization. Locally the gneiss contains metre-scale pods and sheets of amphibolite (some containing relict clinopyroxene), and sub-concordant, metre-scale sheets of variably deformed felsic pegmatite. Epidote mineralisation and the static replacement of amphibole

and biotite by chlorite are indicative of greenschist facies retrogression, with associated local shear band development.

Fugla Ness and North Wick metagabbros and contact relationships with granitic gneiss.

The most common lithology is a medium- to coarse-grained, variably foliated metagabbro composed mainly of an amphibolite facies assemblage of brown-green hornblende and calcic plagioclase. Occasional grains of pyroxene preserved within aggregates of hornblende may be a relic of the original igneous mineralogy. Tectonic strain is low and relict ophitic or sub-ophitic texture is common (Fig. 3b). Evidence for greenschist facies retrogression is provided by the replacement of hornblende by fibrous green mats of actinolite and/or chlorite, and the presence of common epidote and clinozoisite within plagioclase grains. Subordinate lithologies include finer-grained, intermediate metagabbro, coarse-grained hornblendite (Fig. 3c) and pyroxenite, leucogabbro and pegmatite. Contacts between these lithologies can be sharp, but they can also be gradational with marginal intermixing, suggesting the coexistence of different magmas (Fig. 3d). At Fugla Ness an ENE-trending, moderately to steeply dipping foliation defined by aligned amphibole and feldspar aggregates is only locally developed within the central, low strain parts of the body, and more commonly present within 30–40 m of its contacts with the granitic gneiss.

Contacts between the metagabbro and the granitic gneiss are steep and parallel to the ENE-trending foliation in both units. Along the southern margin of the Fugla Ness metagabbro, a 20m wide zone of weakly-deformed sheets of felsic pegmatite separates metagabbro from granitic gneiss. Lenses and pods of undeformed metagabbro up to 2 x 1m in size occur within the pegmatites and are oriented parallel to the contact. The pegmatite and the metagabbro appear to have been contemporaneous melts, both lacking the uniform strong foliation characteristic of the granitic gneiss to the south. In contrast, the northern contact of the metagabbro is characterised by sharply-defined interleaved sheets of granitic gneiss and weakly foliated metagabbro over a total width of *c.* 100 m (Fig. 2). The interleaving varies in scale from tens of metres to 20–30 cm and throughout this zone the granitic gneiss is uniformly foliated, in contrast to the host metagabbro which is typically less strongly deformed. At [HU 3124 9144] weakly deformed metagabbro cuts discordantly across a tight fold of the granitic gneiss (Fig. 3e). This demonstrates clearly that at least some components of the metagabbro were intruded after penetrative deformation of the

granitic gneiss. The central undeformed part of the metagabbro body is intruded by 20–30 cm sheets of undeformed granitic and felsic pegmatite, trending E–W and NE–SW and dipping at angles of >60°. Whether these are late felsic components of the metagabbro intrusion or derived from Devonian plutons *c.* 1 km to the south (Fig. 1) is uncertain.

The interpretation of the relative ages of the granitic gneiss and the Fugla Ness–North Wick metagabbros is not straightforward. It is possible that strain partitioning could account for at least some of the variation in the intensity of fabric development between the two lithologies. However, the field evidence cited above suggests overall that the protolith of the gabbro was intruded *after* the granitic gneiss had acquired its dominant foliation, but *prior to* the cessation of deformation and metamorphism.

Blue Head metagabbro and contact relationships with granitic gneiss.

At Blue Head the granitic gneiss is intruded by a *c.* 75 m wide, steeply-dipping sheet of metagabbro (Fig. 2). This is a relatively homogeneous medium-grained metagabbro, is typically finer-grained and less lithologically variable than the Fugla Ness–North Wick metagabbros. The southern contact with granitic gneiss is faulted locally and marked by concordant quartz–pyrite veins over a width of *c.* 2 m. However, there is no evidence of inter-sheeting of granitic gneiss and metagabbro, and no evidence of net-veining of the latter by felsic sheets. The metagabbro carries a schistose hornblende–feldspar fabric in places, commonly near its margins, but is mostly undeformed and massive. On the map scale, the intrusion trends ESE and dips 80° SSW, significantly oblique to the regional strike and NNW dip of foliation in the host granitic gneiss. It seems unlikely that the localised faulting recorded along the contact can entirely account for this large-scale discordance. The interpretation favoured here is that the metagabbro intruded the granitic gneiss at a later stage in regional deformation and metamorphism. This accounts for the lack of any field relations that might indicate contemporaneity of igneous protoliths and the map-scale structural discordance discussed above. The Blue Head metagabbro is therefore likely to be somewhat younger than the Fugla Ness metagabbro.

Brittle structures

The various brittle structures that affect the Uyea Gneiss Complex comprise early sets of mainly dextral N–S and ENE–WSW strike-slip faults (centimetre to metre scale offsets) and a younger set of NE–SW normal faults with tens of metre scale offsets (Fig. 2).

The Uyea Gneiss Complex in the hanging wall of the Uyea Shear Zone.

The Uyea Shear Zone forms a *c.* 100 m wide zone within which the gneissic foliation in its footwall is progressively reoriented into the southeasterly dip that is characteristic of the hanging wall fabric (Fig. 2). There is no major change in protolith lithology across the shear zone: the hanging wall is dominated by strongly deformed granitoids, from one of which Knudsen (2000) obtained a Nd isotope (T_{DM}) model age of *c.* 2.9 Ga. The hanging wall fabric is blastomylonitic (Fig. 3f) with a variably developed mineral and extension lineation that plunges down-dip to the east-southeast. Kinematic indicators such as shear bands and asymmetrically sheared feldspar porphyroclasts locally show a top-to-the-northwest sense of displacement when viewed on surfaces parallel to the lineation. The widespread ductile recrystallization of feldspar indicates syntectonic temperatures of >450–500˚C (Walker et al. 2016). Rb–Sr white mica ages of *c.* 416 Ma and *c.* 411 Ma from blastomylonites sampled in the hanging wall of the Uyea Shear Zone suggest that it may represent a western front to Caledonian (Scandian) orogenic activity in northwest Shetland (Walker *et al.* 2016).

Locally, N–S trending, undeformed mafic and felsic dykes, mostly <1 m thick, cross-cut the mylonitic gneiss fabrics in the hanging wall of the Uyea Shear Zone. These dykes must be younger than the early Devonian age of the shear zone.

Major and trace element geochemistry

Rock samples were split, passed through a jaw-crusher and powdered in a tungsten carbide Tema mill. Major elements and Sc, Cr, V, Cu, Zn, Ni, Rb, Sr, Y, Zr, Nb, Ba and Pb were analysed by X-ray fluorescence spectrometry, against calibrations defined with international certified reference materials (CRMs). Fusion discs were used for the major elements and pressed powder pellets for trace elements. REEs, Hf, Ta, Th and U were analysed by ICP-MS following fusion dissolutions, also against calibrations defined with international CRMs. Accuracy and precision are monitored with independent CRMs and are estimated to be better than 1% for major elements and 5% for trace elements.

Representative data are listed in Table 1 and results are summarised in plots on Fig. 4. The data define a coherent geochemical suite with significant elemental variation. The total alkalis versus silica (TAS) plot (Fig. 4a) demonstrates the extended compositional range, from gabbro and monzogabbro to granodiorite and granite. Mafic enclaves in the granitic gneisses plot close to the metagabbro bodies in this and other major element

diagrams (not shown). Hornblendite layers from the metagabbro bodies plot within the gabbro field, but have distinct geochemistry exemplified by relatively high MgO, Cr and Ni with low Al_2O_3 (Table 1). The mafic orthogneisses have low Cr and Ni (generally significantly below 100 ppm) that suggest pre-emplacement mafic mineral fractionation assuming a mantle source. The AFM diagram (Fig. 4b) shows a clear calc-alkaline affinity, with continuous variation even within this small dataset. REE data (Fig. 4c) define an extensive range of light-REE enriched patterns, with variable Eu anomalies from large and negative in the high-REE samples, to small and positive in some of the low-REE samples. There is a strong correlation between total REE concentration and P_2O_5 among all samples (not shown, but evident in Table 1). The relatively low REE group contains hornblendites, mafic and felsic orthogneisses, all of which show moderate light-REE enrichment with the progressive development of a small positive Eu anomaly and concave-upward heavy REEs in the felsic orthogneiss samples. Both the latter features are consistent with amphibole fractionation, possibly represented by the hornblendites. The mantle-normalized multi-element diagram for the latter rocks (i.e. excluding the high P_2O_5 group, Fig. 4d) shows all the characteristics of subduction-related magmatism; strong enrichment in fluid-mobile large-ion lithophile elements (e.g. Rb, Ba, U and K) towards the left of the diagram, a significant Nb-Ta trough and a distinct peak at Pb. Importantly, the mafic and felsic orthogneiss patterns are very similar, consistent with a genetic relationship between them.

U–Pb Geochronology

Three samples of granitic gneiss from the western coastal section, and three of the Fugla Ness metagabbro were obtained for a combined U–Pb zircon geochronological and Hf isotope study aimed at establishing the ages and constraining the sources of their igneous protoliths. An additional granitic gneiss sample (SH12-006) was obtained from above the Uyea Shear Zone to test the interpretation that these orthogneisses represent the reworked equivalent of those in its footwall. Sample localities are shown in Fig. 2. Zircon grains were separated for analysis from 2–3 kg crushed rock samples by standard density and magnetic separation methods. Representative zircon cathodoluminescence (CL) images of sectioned zircons are shown in Fig. 5. A sample of the Blue Head metagabbro unfortunately did not yield any zircon.

The zircons separated from the three coastal granitic gneiss samples were similar in appearance. Generally, these were light brown, subhedral tetragonal prisms up to 200 µm long. Under CL imaging (Fig. 5a), most grains displayed magmatic-style oscillatory internal zonation. Some grains had, in addition, a uniform outer rim, the boundary of which partly encroached upon interior zones, implying partial resorption (e.g. SH12-007 grains 3 and 6, Fig. 5a). A minority had a distinct, either irregularly zoned, sector zoned or uniform central core (e.g. SH12-022 grain 16, Fig. 5a). Granitic gneiss sample SH12-006 from east of the Uyea Shear Zone yielded sub- to anhedral zircon grains, generally displaying magmatic-style oscillatory zonation. Similar to the zircons from the coastal samples, some grains had distinct structural cores and some had distinctly discordant outer layers.

The zircons from the three metagabbro samples from Fugla Ness showed less regularity in shape and internal zonation than those from the felsic rocks. Most were pink coloured, subhedral prismatic grains and grain fragments, some up to 250 µm in size. Generally they lacked fine scale oscillatory zonation, but rather had broader growth zones combined with sector and more irregular zonation features (Fig. 5b). A few grains had outer zones that could possibly be interpreted as later-added or modified rims, including irregularly-bounded areas encroaching upon grain interiors that appear to represent areas of recrystallization (e.g. S05-10 grain 16 and SH12-008 grain 12, Fig. 5b). Another difference from the granitic gneiss zircons was that distinct structural cores were not observed in these samples.

U–Pb isotopic compositions were measured in two analytical sessions using a Sensitive High Resolution Ion Microprobe (SHRIMP II) at the John de Laeter Centre, Perth, Western Australia. Grains were mounted in polished and gold-coated epoxy resin discs together with chips of reference zircons. Analytical procedures were based on those outlined initially by Compston *et al*. (1984). The SHRIMP II was operated at a mass resolution of 5000 using a primary beam current of 1.5–2 nA and target spot diameter of 20–25 µm. Common Pb was corrected using the measured ^{204}Pb isotope in each sample and modelled on Broken Hill Pb composition. For most analyses, the size of the correction to the ^{206}Pb counts was less than 1% (see %common ^{206}Pb in Table 2).

The observed co-variance between Pb^+/U^+ and UO^+/U^+ obtained from analyses of the reference zircons was used to correct instrumental inter-element discrimination of Pb/U ratios. In the first analytical session in which samples S05-10 and S05-11 were run,

reference zircon CZ3 (Mean $^{206}Pb/^{238}U$ age = 561.5 Ma, Nasdala et al. 2008) was used as the primary Pb/U standard, while grains of OGC-1 ($^{207}Pb/^{206}Pb$ age = 3465 Ma, Stern et al. 2009) were used to monitor $^{207}Pb/^{206}Pb$ ratios for possible Pb isotope mass fractionation. For this session, six analyses of OGC-1 yielded a mean ^{204}Pb-corrected $^{207}Pb/^{206}Pb$ age of 3467 ± 13 Ma, so no calibrated correction to Pb/Pb ratios of unknowns was applied. In the second analytical session, reference zircon BR266 ($^{206}Pb/^{238}U$ age = 559.0 Ma, Stern 2001) was used as the primary Pb/U standard, Temora-2 ($^{206}Pb/^{238}U$ age = 416.8 Ma, Black et al. 2004) as a secondary Pb/U standard and again OGC-1 to monitor Pb/Pb ratios for fractionation. In this session the calculated mean $^{207}Pb/^{206}Pb$ age for analyses of OGC-1 was 3461 ± 4 Ma and the mean radiogenic $^{206}Pb/^{238}U$ age of Temora-2 was 416 ± 6 Ma. All data were processed using SQUID and Isoplot/Ex software (Ludwig 2001, 2009). Uncertainties of combined mean ages are quoted at 95% confidence limits.

Results – Granitic gneisses

The results of the individual zircon U–Pb spot analyses are listed in Table 2 and summarised on Tera-Wasserburg concordia plots in Fig. 6 as one sigma error ellipses. Most analyses yielded data less than 5% discordant, defined here as the percentage difference between the measured radiogenic $^{206}Pb/^{238}U$ and $^{207}Pb/^{206}Pb$ ages. Analyses of oscillatory zoned regions of the grain interiors representing the main phase of magmatic crystallization produced clusters of approximately concordant analyses shown in red in Fig. 6a. These were combined to estimate intrusion ages for the samples based on their weighted mean $^{207}Pb/^{206}Pb$ ratios calculated using Isoplot/Ex. By this method, coastal sample S05-11 yielded a magmatic age of 2741.4 ± 5.4 Ma (2σ, MSWD = 1.4), while samples SH12-007 and SH12-022 yielded similar results of 2745.9 ± 4.8 Ma (MSWD = 2.4) and 2744.7 ± 7.2 Ma (MSWD = 3.3), respectively.

Some distinctly older structural cores were found among the mounted zircons from all three of the coastal granitic gneiss samples, shown in green shading in Fig. 6a. These yielded individual $^{207}Pb/^{206}Pb$ ages ranging from 2763 ± 9 to 2811 ± 19 Ma (1σ errors), with too much scatter to be considered as a single age population, but likely indicating a narrow age range of older crust through which the granitic magmas intruded. Conversely, analyses of distinct rims of uniform appearance on some of the zircons in samples SH12-007 and SH12-022 yielded younger $^{207}Pb/^{206}Pb$ ages than the main magmatic populations (analyses

shown in blue on Fig. 6a). The weighted average of three rim analyses in SH12-007 produced an age estimate for these of 2713 ± 12 Ma (2σ, MSWD = 1.1).

During analysis of sample SH12-006 from the hanging wall (eastern side) of the Uyea Shear Zone, increasing SHRIMP primary beam instability was encountered, as a result of which only a few publishable analyses were obtained (Table 2). The three analyses that were less than 5% discordant combine to a weighted mean $^{207}Pb/^{206}Pb$ age of 2737.0 ± 5.9 Ma (2σ, MSWD = 0.9), i.e. similar to the results from the footwall samples, in spite of the textural evidence for Caledonian reworking of this gneiss sample.

Results – Fugla Ness metagabbro

The results of individual spot analyses of the zircons from the three Fugla Ness metagabbro samples are shown on concordia plots in Fig. 6b, see also Table 2. As for the granitic gneiss samples, the majority of analyses of the variably zoned grain interiors, shaded red on Fig. 6b and interpreted as of magmatic origin, plot within 5% of the concordia curve. Using Isoplot/Ex, these were combined to yield weighted mean $^{207}Pb/^{206}Pb$ ages as follows: Sample S05-10, mean $^{207}Pb/^{206}Pb$ age 2729.6 ± 7.7 Ma (2σ, MSWD = 2.2); sample SH12-019 mean $^{207}Pb/^{206}Pb$ age 2726.3 ± 7.8 Ma (MSWD = 1.9); sample SH12-008 mean $^{207}Pb/^{206}Pb$ age 2737.4 ± 3.7 Ma (MSWD = 1.5).

Among the zircons analysed from the metagabbro, no distinctly older structural cores were identified. There were, however, a few areas of evidently recrystallized/added zircon which truncated the magmatic zonation of the grain interiors (analyses shown in blue, Fig. 6b). Two such areas in sample S05-10 yielded a combined $^{207}Pb/^{206}Pb$ age of 2703 ± 17 Ma (2σ), similar to the 2713 ± 14 Ma $^{207}Pb/^{206}Pb$ age obtained from spot 12.2 in sample SH12-008.

Hafnium Isotope Analysis

Hf isotope analysis of selected zircons was carried out using a Merchantek EO LUV laser-ablation microprobe attached to a Nu Plasma multi-collector inductively coupled plasma mass spectrometer at GEMOC, Macquarie University, New South Wales (Griffin et al. 2000). Pits of approximately 50 µm diameter and 40 µm depth, overlapping the smaller SHRIMP U–Pb analytical sites, were produced by the 213 nm Nd:YAG laser. A 5 Hz repetition with energies of 0.12 – 0.15 mJ per pulse resulted in Hf signals of 1 to 6 $\times 10^{-11}$ A over the 200 to 250 second ablation intervals. The ablated material was transported to the ICP-MS torch by

He carrier gas. Hf isotopes were measured simultaneously on Faraday Cups in static-collection mode.

Data were normalized to $^{179}Hf/^{177}Hf = 0.7325$ using an exponential correction for mass fractionation. Interference by ^{176}Lu on ^{176}Hf was corrected via measurement of ^{175}Lu, using $^{176}Lu/^{175}Lu = 0.02669$; interference by ^{176}Yb on ^{176}Hf was corrected via measurement of ^{172}Yb, using $^{176}Yb/^{172}Yb = 0.5865$, the latter determined through spiking of the JMC475 hafnium standard solution with ytterbium and then finding the Yb ratio required to yield the $^{176}Hf/^{177}Hf$ value for the unspiked solution (Griffin et al. 2000). Reference zircons Mud Tank and 91500 were analysed at intervals with the unknowns to monitor the accuracy and precision of the corrected $^{176}Hf/^{177}Hf$ ratios. The typical 2σ precision on individual $^{176}Hf/^{177}Hf$ ratios was ± 0.000015, equivalent to ± 0.5 εHf units (Table 3).

Results – Granitic gneisses

Hf isotopic data for zircons from three of the granitic gneiss samples: SH12-007, SH12-022 and SH12-006, are listed in Table 3 and plotted on a Hf evolution diagram in Fig. 7 at their indicated $^{207}Pb/^{206}Pb$ age. Grain-spot numbers listed in Table 3 correspond to original SHRIMP grain-spot numbers in Table 2. All Hf laser spots were located in zones of magmatic crystallization (red points, Fig. 7), except for three analyses in older cores (SH12-007 spots 7.1, 12.1 and 16.1 - blue points, Fig. 7). The three granite gneiss samples, including SH12-006 from east of the Uyea Shear Zone, yielded similar results, with the range of $^{176}Hf/^{177}Hf$ ratios corresponding to εHf values of –2.0 to +0.5, average –0.5. Using these values, an assumed depleted mantle source for the crustal precursor rocks, and an estimated $^{176}Lu/^{177}Hf$ ratio of 0.009 for those original rocks (Gardiner et al. 2018), mantle extraction T_{DM} model ages of between *c.* 3.2 and 3.1 Ga were calculated.

Results – Fugla Ness metagabbro

Selected zircons from two of the metagabbro samples: SH12-008 and SH12-019 were analysed (Table 3). The results are plotted as green points on Fig. 7. The range of measured Hf compositions overlaps with those of the granitic gneisses but extends to more positive εHf values. The recorded range was from –1.2 to +3.0, average +0.5, from which (two-stage) mantle extraction T_{DM} model ages of between *c.* 3.2 and 3.0 Ga were calculated.

Discussion

Age of the Uyea Gneiss Complex

The zircon U–Pb ages reported here confirm that the igneous protoliths of the Uyea Gneiss Complex on Shetland crystallized in the Neoarchaean between c. 2746 Ma and c. 2726 Ma ago, with a few older cores in the granitic gneiss samples up to c. 2811 Ma old. The protolith age of the granitic gneiss sampled from above the Uyea Shear Zone (USZ) lies within error of the ages determined for the same lithology in its footwall. This supports the view that the USZ has reworked lithologies belonging to the same meta-igneous complex (Pringle 1970; Flinn 2009) and it does not therefore represent a fundamental tectonic boundary. The intrusion ages of the Fugla Ness metagabbro are systematically younger than those obtained from the granitic gneisses, although partly overlapping in their analytical uncertainty. This is consistent with the field evidence that the Fugla Ness metagabbro is the younger of the two units while the overall close similarity in age of the mafic and felsic units supports the geochemical evidence that they are genetically related, albeit not via a simple liquid line of descent. An additional event affecting the complex at c. 2713 Ma is indicated by distinct rims on, and recrystallized areas within, some zircons from both the granite gneisses and metagabbro samples. This might represent the tectonothermal event responsible for the amphibolite facies ductile fabrics and the modified contacts between the lithologies.

Comparison with the Cullivoe basement inlier, Yell

The only other verified occurrence of Archaean rocks on Shetland is the Cullivoe inlier that forms a narrow strip on the northeastern edge of the island of Yell (Fig. 1) and extending south to the neighbouring island of Hascosay. This inlier comprises generally highly strained hornblendic and felsic orthogneisses that are in tectonic contact with younger metasedimentary units of the Yell Sound and Westing Groups (Flinn 1988, 2009; Jahn et al. 2017). Unlike the zircons from the Uyea gneisses analysed here, those from the Cullivoe inlier have been strongly affected by a Neoproterozoic (c. 940 Ma) high-grade metamorphic event that caused substantial Pb loss (Jahn et al. 2017). This event had been documented previously in rocks east of the Walls Boundary Fault by Cutts et al. (2009, 2011). Based on the least disturbed analyses, Jahn et al. reported protolith age estimates of c. 2820 Ma for a felsic orthogneiss and c. 2700 Ma for a metagabbro on the Migga Ness peninsula, both with large uncertainties. Those results are in broad agreement with the more precise ages

obtained here for the Uyea gneisses. Furthermore, some of the Cullivoe orthogneisses have geochemical characteristics (light-REE enrichment, small positive Eu anomalies, concave-upward heavy REE patterns) that are similar to those of the Uyea felsic orthogneisses, and which suggest TTG suite affinity (Jahn et al. 2017). However, the mafic rocks at Cullivoe are significantly different, being tholeiitic, mildly light-REE depleted and higher in heavy REE abundances (Jahn et al. 2017).

Comparison with offshore borehole data

Extensive drilling beneath the North Sea has revealed that Archaean basement rocks occupy a ≥ 550 km tract of the U.K. continental shelf stretching from north of mainland Scotland and the Outer Hebrides to the north and west of Shetland. Chambers et al. (2005) showed that granodioritic to dioritic, amphibolite facies gneisses with TTG affinity occur along this tract in two main age groupings: an older group with zircon U–Pb crystallization ages of c. 2830 to c. 2800 Ma and a younger group c. 2740 to c. 2700 Ma with some older inheritance (representative ages shown in Fig. 8). Two-stage whole-rock Nd T_{DM} model ages for the dated samples range from 3.02 to 2.94 Ga (Chambers et al. 2005). Similar age groupings were reported recently by Holdsworth et al. (2019) for an offshore data set of granitic and granodioritic gneisses with an overall age range of c. 2860 to c. 2700 Ma. Holdsworth et al. (2019) also reported zircon Hf T_{DM} model ages in the range 3.25 to 2.90 Ga. The data set of Chambers et al. (2005) included samples with granulite facies assemblages, but neither study reported evidence for high-grade reworking of the dated samples nor for significant ancient Pb loss during the Proterozoic Era or earlier. Thus these offshore samples show broad similarity to the Uyea Gneiss Complex in terms of age, isotopic characteristics and post-crystallization history, which is consistent with them belonging to the same structural domain: the Faroe–Shetland Block of Richie et al. (2011).

Correlation with the Lewisian Gneiss Complex

The new data reported here provide a firm basis for assessing the proposed correlation of the Uyea Gneiss Complex on Shetland with the Lewisian Gneiss Complex of mainland Scotland and the Outer Hebrides (Flinn et al. 1979; Flinn 1985). Compiled zircon data from the various sub-divisions of the Lewisian Gneiss Complex indicate that most of its principal TTG components have protolith ages of c. 2800 to c. 2900 Ma (Fig. 7), with some Assynt terrane protoliths dating back further to c. 3000 Ma (Kinny et al. 2005; Wheeler et al. 2010

and references therein). Several 'Lewisian-like' Moine inlier protoliths date from c. 2800 to c. 2900 Ma also (Friend et al. 2008), as does the Cullivoe inlier orthogneiss on Yell dated by Jahn et al. (2017) and some of the older offshore borehole samples reported by Chambers et al. (2005) and Holdsworth et al. (2019). Not represented on Fig. 7 are two earlier, c. 3130 Ma components of the Lewisian Gneiss Complex identified on the Outer Hebrides island of Harris (Friend & Kinny 2001) and from Loch Torridon on the mainland (Love et al. 2010). The c. 2746 Ma to c. 2726 Ma period of crystallization of the Uyea Gneiss Complex thus post-dates the main crystallization phase of TTG gneisses in the Lewisian Gneiss Complex and correlated inliers on the Scottish mainland by some tens of millions of years. On the other hand, parts of the Lewisian Gneiss Complex do record high-grade metamorphism during this interval (Fig. 7), notably the Gruinard terrane at c. 2730 Ma (Love et al. 2004) and arguably the Assynt terrane as well (e.g. Crowley et al. 2015), though the latter was strongly affected by a further episode of high-grade metamorphism at c. 2500 Ma that has significantly obscured its earlier history. Based on age relationships alone, the Uyea Gneiss Complex can therefore be regarded as a late addition to the Meso- to Neoarchaean Lewisian Gneiss Complex.

The Hafnium isotopic compositions of the Uyea Gneiss Complex zircons provide a further point of comparison with the Lewisian Gneiss Complex. The initial epsilon Hf values of both the mafic and felsic units at their time of crystallization are clustered around zero ('chondritic'), at a time when the average depleted mantle is modelled to have had an εHf of +7 (Fig. 7). At +0.5, the average εHf for the mafic units is only one epsilon unit higher than the corresponding average value for the felsic units (–0.5). Similar values were obtained from one group of the offshore felsic gneiss samples studied by Holdsworth et al. (2019), while a second group had lower εHf values clustered at c. –4.0. As shown on Fig. 7, similar ranges in εHf have been measured in zircons from TTG gneisses of the Gruinard and Assynt terranes of the Lewisian Gneiss Complex (Love 2003; Whitehouse & Kemp 2010), such that the older Lewisian protolith compositions lie along the projected Hf evolution path through which the precursor rocks to the Uyea Gneiss Complex could have evolved. This is not to say that the felsic Uyea gneisses necessarily represent reworked Lewisian TTG protoliths, but rather that all plausibly developed in a series of melting events affecting juvenile, presumably basaltic crust that separated from the mantle c. 3.0 to 3.2 Ga ago, as indicated by their two-stage Hf model ages (Table 3, Holdsworth et al. 2019). On the other hand, the

Uyea Gneiss Complex presents a perhaps unique situation in the region insofar as it comprises metabasic intrusions of calc-alkaline affinity that are evidently mantle-derived together with broadly coeval felsic units that appear geochemically to share a common origin. The geochemical evidence, therefore, suggests that the entire complex represents a new addition to the crust rather than reworked older crust.

The ultimate source of this new crust is another question. One way to explain εHf values close to zero at the time of emplacement is a source from residual undepleted mantle, however this seems unlikely as straightforward melting of such a source would not produce the observed geochemical signatures. The alternative is an enriched mantle source, of the kind that would be generated in an arc environment where subduction of hydrated basaltic crust is operating. Such a melting environment would more readily explain the relative enrichments of Rb, Ba, U over Th, LREE. Either way, it follows that the Hf model ages are not meaningful as crustal extraction ages in this case, as they presuppose a depleted mantle source. The slightly more negative εHf of the felsic gneisses and the presence of zircon cores with ages up to c. 2810 Ma are consistent with a limited interaction of the differentiated magmas with relatively young, pre-existing crust during ascent and emplacement.

Many of the TTG rocks in the Lewisian Complex have 'arc-like' trace element signatures, although it has also been suggested that such signatures may relate to processes such as delamination and dripping rather than subduction (Johnson et al. 2016). However, the Lewisian and TTG-dominated Archaean gneiss complexes elsewhere generally lack coeval, genetically-related mafic rocks. One occurrence in the Lewisian of an inclusion suite interpreted as coeval to the TTG magmas is in the Gruinard Terrane where hornblendite–metagabbro bodies occur in trondhjemite-hosted agmatite (Whitehouse et al., 1996). More typically these complexes contain dismembered inclusions that geochemically resemble the products of fractionated tholeiitic magmas, e.g. the abundant layered mafic–ultramafic bodies in the Assynt terrane of the Lewisian (Johnson et al. 2016), the main amphibolite suite in the Gruinard Terrane (Whitehouse et al., 1996) and the mafic gneisses of the Cullivoe inlier on Yell (Jahn et al. 2017).

Another key point of difference between the Uyea and Lewisian Gneiss Complexes is their contrasting post-crystallization histories. In the (admittedly limited) area of exposure of the Uyea Gneiss Complex, there is no equivalent to the Scourie dyke swarms that

crosscut the Archaean components of the Lewisian Gneiss Complex. Nor are there any identified shear zones dating from the c. 2490 Ma 'Inverian' event of mainland Scotland, nor from the later Palaeoproterozoic 'Laxfordian' period of reworking of much of the Lewisian Gneiss Complex. Additionally, there is no evidence for the c. 1875 Ma granulite facies metamorphism that affected the igneous complex and adjacent metasedimentary belts of South Harris in the Outer Hebrides (Whitehouse & Bridgwater 2001), nor for any other Proterozoic high-grade events recorded in various parts of the assembled Lewisian Gneiss Complex. Aside from the c. 2710 Ma zircon rims and the ductile fabrics of the Uyea Gneiss Complex that may relate to an early deformation event, there is no evidence for any further significant tectonothermal activity affecting the Uyea complex until the Caledonian. Chambers et al. (2005) and Holdsworth et al. (2019) noted a similar lack in evidence for post-Archaean reworking of the proximal offshore samples as well. The reason for this difference may be the more northerly location of Shetland compared to the rest of the U.K., as discussed below.

Regional correlations and linkages with East Greenland

The many similarities between the geology of the Lewisian Gneiss Complex and the Nagssugtoqidian Orogen of Greenland have led numerous previous authors (e.g. Kalsbeek et al. 1993; Friend & Kinny 2001; Park 2005) to conclude that they were contiguous prior to the opening of the North Atlantic Ocean (Fig. 8). Both record similar ranges of Meso- to Neoarchaean protolith and metamorphic ages, and both were strongly reworked and intruded by igneous complexes during a similar interval of the Palaeoproterozoic Era. In Greenland, the Nagssugtoqidian Orogen is argued to have developed at the southern margin of the Rae Craton by northward accretion of microcontinents c. 1880–1865 Ma, followed by collision of the Rae and North Atlantic cratons c. 1860–1840 Ma (St-Onge et al. 2009; Garde & Hollis 2010; Kolb 2014). In East Greenland, the Nagssugtoqidian Orogen is bounded to the north by a foreland consisting of predominantly granulite facies Archaean rocks of the Rae Craton (Nutman et al. 2008). Although the geology of this remote part of East Greenland is relatively poorly known, the available evidence suggests that the Rae Craton was a stable cratonic block during the Palaeoproterozoic (Nutman et al. 2008). The map reconstruction in Fig. 8 places the coastal exposures of the Rae Craton in East Greenland opposite Shetland, and the apparent absence of Palaeoproterozoic reworking of

the Uyea Gneiss Complex and of the offshore basement west of Shetland supports the idea that these segments of crust were once connected. If this is so, the eastern extension of the northern boundary of the Nagssugtoqidian Orogen must lie between Shetland and mainland Scotland, more specifically between the southernmost of the sampled boreholes (North Rona Basin) and mainland Scotland (Fig. 8).

Conclusions

1) The Uyea Gneiss Complex of northern Shetland is dominated by granitic gneiss and syn- to late-kinematic metagabbro bodies. U–Pb dating of zircon indicates that the igneous protoliths crystallized between c. 2746 Ma and c. 2726 Ma ago, with the indicated crystallization ages of the metagabbros marginally younger than those of the granitic gneisses, albeit with some overlap in analytical uncertainty.
2) The Uyea shear zone that divides the complex does not appear to represent a fundamental tectonic boundary, as samples of gneiss from both sides have similar protolith ages. Rather it marks the western limit of Caledonian reworking. West of the Uyea shear zone, the granitic gneiss and metagabbros carry a similarly-oriented deformation fabric, with amphibolite facies textures and mineralogies. Based on the ages of zircon rims/recrystallized areas, these features possibly developed c. 2710 Ma, i.e. soon after their initial emplacement.
3) Both the granitic gneisses and metagabbros have calc-alkaline geochemistry that is sufficiently similar to suggest a genetic kinship. Their mantle-normalized trace element abundances strongly suggest a common arc-related origin. Zircon εHf values range from –2.0 to +0.5 (granitic gneisses) and –1.2 to +3.0 (metagabbros) at their indicated crystallization ages, and imply an enriched mantle source. Minor zircon inheritance in the granitic gneisses suggests limited interaction with older crustal sources.
4) The c. 2746–2726 Ma period of development of the Uyea Gneiss Complex post-dates the main crystallization phase of the Lewisian Gneiss Complex on the Scottish mainland by some tens of millions of years, but coincides with a time when parts of the complex underwent high-grade metamorphism. Similar Neoarchaean protolith ages obtained from offshore basement drill core samples north and west of the

Shetland Islands support the Uyea Gneiss Complex being grouped in the same structural domain, termed the Faroe–Shetland Block by Richie et al. (2011).

5) Unlike the Lewisian Gneiss Complex and correlated rocks of the Nagssugtoqidian Orogen of East Greenland, neither the Uyea Gneiss Complex nor its equivalent offshore basement appear to have experienced significant Palaeoproterozoic ('Laxfordian') reworking. This is consistent with their more northerly position prior to opening of the North Atlantic Ocean that suggests they were once connected to the Archaean Rae Craton. This would place the continuation of the northern boundary of the Nagssugtoqidian Orogen between Shetland and the Scottish mainland.

Acknowledgments

Mark Witton is thanked for drafting Figures 1, 2 and 8. Our thanks also to Fernando Corfu and Martin Whitehouse for their thoughtful reviews of an earlier version of this paper, and to Stephen Daly for editorial handling.

References

Black, L.P., Kamo, S.L., Allen, C.M., Davis, D.W., Aleinikoff, J.N., Valley, J.W., Mundil, R., Campbell, I.H., Korsch, R.J., Williams, I.S. & Foudoulis, C. 2004. Improved $^{206}Pb/^{238}U$ microprobe geochronology by the monitoring of a trace-element-related matrix effect; SHRIMP, ID-TIMS, ELA-ICP-MS, and oxygen isotope documentation for a series of zircon standards. *Chemical Geology,* **205**, 115-140.

Blichert-Toft, J. & Albarède, F. 1997. The Lu-Hf isotope geochemistry of chondrites and the evolution of the mantle-crust system. *Earth and Planetary Science Letters*, **148**, 243-258.

Chambers, L., Darbyshire, F., Noble, S. & Ritchie, D. 2005. NW UK continental margin: chronology and isotope geochemistry. *British Geological Survey Commissioned Report*, CR/05/095.

Compston, W., Williams, I.S. & Meyer, C. 1984. U–Pb Geochronology of Zircons from Lunar Breccia 73217 Using a Sensitive High Mass-Resolution Ion Microprobe. *Journal of Geophysical Research,* **89**, Supplement B, 525-534.

Crowley, Q.G., Key, R. & Noble, S.R. 2015. High-precision U–Pb dating of complex zircon from the Lewisian Gneiss Complex of Scotland using an incremental CA-ID-TIMS approach. *Gondwana Research*, **27**, 1381-1391.

Cutts, K.A., Hand, M., Kelsey, D.E., Wade, B., Strachan, R.A., Clark, C. & Netting, A. 2009. Evidence for 930 Ma metamorphism in the Shetland Islands, Scottish Caledonides: implications for Neoproterozoic tectonics in the Laurentia–Baltica sector of Rodinia. *Journal of the Geological Society*, *London,* **166**, 1033-1048.

Cutts, K.A., Hand, M., Kelsey, D. E. & Strachan, R.A. 2011. P–T constraints and timing of Barrovian metamorphism in the Shetland Islands, Scottish Caledonides: implications for the structural setting of the Unst ophiolite. *Journal of the Geological Society, London*, **168**, 1265-1284.

Davies, J.H.F.L. & Heaman, L.M. 2014. New U–Pb baddeleyite and zircon ages for the Scourie dyke swarm: a long-lived large igneous province with implications for the Palaeoproterozoic evolution of NW Scotland. *Precambrian Research*, **249**, 180-198.

Flinn, D. 1985. The Caledonides of Shetland. *In*: Gee, D.G. & Sturt, B.A. (eds) *The Caledonide Orogen Scandinavia and Related Areas*. Wiley & Sons, New York, 1159-1172.

Flinn, D. 1988. The Moine rocks of Shetland. *In*: Winchester, J.A. (ed.) *Later Proterozoic Stratigraphy of the Northern Atlantic Regions*. Blackie, Glasgow, 74-85.

Flinn, D. 2009. Lewisian and Moine of Shetland. *In:* Mendum, J.R., Barber, A.J., Butler, R.W.H., Flinn, D., Goodenough, K.M., Krabbendam, M., Park, R.G. & Stewart, A.D. (eds) *Lewisian, Torridonian and Moine Rocks of Scotland*. Geological Conservation Review Series, **34**, Joint Nature Conservation Committee, Peterborough, 623-650.

Flinn, D., Frank, P.L., Brook, M. & Pringle, I.R. 1979. Basement–cover relations in Shetland. *In*: Harris, A.L., Holland, C.H. & Leake, B.E. (eds) *The Caledonides of the British Isles - Reviewed*. Geological Society, London, Special Publications, **8,** 109-115.

Friend, C.R.L. & Kinny, P.D. 2001. A reappraisal of the Lewisian Gneiss Complex: geochronological evidence for its tectonic assembly from disparate terranes in the Proterozoic. *Contributions to Mineralogy and Petrology*, **142**, 198-218.

Friend, C.R.L., Strachan, R.A. & Kinny, P.D. 2008. U–Pb zircon dating of basement inliers within the Moine Supergroup, Scottish Caledonides: implications of Archaean protolith ages. *Journal of the Geological Society, London,* **165**, 807-815.

Garde, A.A. & Hollis, J.A. 2010. A buried Palaeoproterozoic spreading ridge in the northern Nagssugtoqidian orogen, West Greenland. *In*: Kusky, T., Zhai, M-G & Xiao, W. (eds), *The Evolving Continents: Understanding Processes of Continental Growth*. Geological Society, London, Special Publications, **338**, 213-234.

Gardiner, N.J., Johnson, T.E., Kirkland, C.L. & Smithies, R.H. 2018. Melting controls on the lutetium-hafnium evolution of Archaean crust. *Precambrian Research* **305**, 479-488.

Goodenough, K.M., Crowley, Q.C., Krabbendam, M. & Parry, S.F. 2013. New U–Pb age constraints for the Laxford Shear Zone, NW Scotland: evidence for tectonomagmatic processes associated with the formation of a Palaeoproterozoic supercontinent. *Precambrian Research*, **233**, 1-19.

Griffin, W.L., Pearson, N.J., Belousova, E., Jackson, S.E., O'Reilly, S.Y., van Achterberg, E. & Shee, S.R. 2000. The Hf isotope composition of cratonic mantle: LAM-MC-ICPMS analysis of zircon megacrysts in kimberlites. *Geochimica et Cosmochimica Acta* **64**, 133-147.

Holdsworth, R.E., Morton, A., Frei, D., Gerdes, A., Strachan, R.A., Dempsey, E., Warren, C. & Whitham, A. 2019. The nature and significance of the Faroe–Shetland Terrane: Linking Archaean basement blocks across the North Atlantic. *Precambrian Research*, **321**, 154–171.

Jahn, I., Strachan, R.A., Fowler, M.B., Bruand, E., Kinny, P.D., Clark, C. & Taylor, R.J.M. 2017. Evidence from U–Pb zircon geochronology for early Neoproterozoic (Tonian) reworking of an Archaean inlier in northeastern Shetland, Scottish Caledonides. *Journal of the Geological Society, London,* **174**, 217-232.

Johnson, T.E., Brown, M., Goodenough, K.M., Clark, C., Kinny, P.D. & White, R.W. 2016. Subduction or sagduction? Ambiguity in constraining the origin of ultramafic–mafic bodies in the Archean crust of NW Scotland. *Precambrian Research*, **283**, 89–105.

Kalsbeek, F., Austrheim, H., Bridgwater, D., Hansen, B.T., Pedersen, S. & Taylor, P.N. 1993. Geochronology of Archaean and Proterozoic events in the Ammassalik area, South-East

Greenland, and comparisons with the Lewisian of Scotland and the Nagssugtoqidian of West Greenland. *Precambrian Research,* **62**, 239-270.

Kinny, P.D. & Friend, C.R.L. 1997. U–Pb isotopic evidence for the accretion of different crustal blocks to form the Lewisian Complex of northwest Scotland. *Contributions to Mineralogy and Petrology*, **129**, 326-340.

Kinny, P.D., Friend, C.R.L. & Love, G.J. 2005. Proposal for a terrane-based nomenclature for the Lewisian Gneiss Complex of NW Scotland. *Journal of the Geological Society, London*, **162**, 175-186.

Knudsen, T-L. 2000. The provenance of Devonian sandstones from Shetland: a Sm–Nd and trace element study. *Scottish Journal of Geology*, **36**, 61-72.

Kolb, J. 2014. Structure of the Palaeoproterozoic Nagssugtoqidian Orogen, South-East Greenland: Model for the tectonic evolution. *Precambrian Research*, **255**, 809-822.

Love, G.J. 2003. The Origin and Accretionary Development of the Lewisian Gneiss Complex of NW Scotland: Constraints from *in situ* U–Pb and Hf Isotopic Analysis of Accessory Minerals. PhD Thesis, Curtin University.

Love, G.J., Kinny, P.D. & Friend, C.R.L. 2004. Timing and magmatism and metamorphism in the Gruinard Bay area of the Lewisian Gneiss Complex: comparisons with Assynt Terrane and implications for terrane accretion. *Contributions to Mineralogy and Petrology,* **164**, 620-636.

Love, G.J., Friend, C.R.L. & Kinny, P.D. 2010. Palaeoproterozoic terrane assembly in the Lewisian Gneiss Complex on the Scottish mainland, south of Gruinard Bay: SHRIMP U–Pb zircon evidence. *Precambrian Research,* **183**, 89-111.

Ludwig, K.R. 2003. Isoplot 3.00; A Geochronological Toolkit for Microsoft Excel. Berkeley Geochronology Centre, Berkeley, California, USA, Special Publication 4, 70pp.

Ludwig, K.R. 2009. Squid 2.50, A User's Manual. Berkeley Geochronology Centre, Berkley, California, USA, Unpublished Report, 95pp.

Mason, A.J. 2012. Major early thrusting as a control on the Palaeoproterozoic evolution of the Lewisian Complex: evidence from the Outer Hebrides, NW Scotland. *Journal of the Geological Society, London*, **169**, 201-212.

Nasdala, L., Hofmeister, W., Norberg, N., Mattinson, J.M., Corfu, F., Dörr, W., Kamo, S.L., Kennedy, A.K., Kronz, A., Reiners, P.W., Frei, D., Kosler, J., Wan, Y., Götze, J., Häger, T., Kröner, A. & Valley, J.W. 2008. Zircon M257 – a homogeneous natural reference material for the ion microprobe U–Pb analysis of zircon. *Geostandards and Geoanalytical Research,* **32**, 247-265.

Nutman, A.P., Kalsbeek, F. & Friend, C.R.L. 2008. The Nagssugtoqidian orogen in South-West Greenland: evidence for Palaeoproterozoic collision and plate assembly. *American Journal of Science*, **308**, 529-572.

Park, R.G. 2005. The Lewisian terrane model: a review. *Scottish Journal of Geology*, **41**, 105-118.

Pringle, I.R. 1970. The structural geology of the North Roe area of Shetland. *Geological Journal.* **7**, 147-170.

Ritchie, J.D., Noble, S., Darbyshire, F. Millar, I. & Chambers, L. 2011. Pre-Devonian. *In*: Ritchie, J.D., Ziska, H., Johnson, H. & Evans, D. (eds) *Geology of the Faroe–Shetland Basin and adjacent areas.* British Geological Survey Research Report, RR/11/01, Jarôfeingi Research Report, RR/11/01, 71-78.

Robinson, T. 1983. Basement–cover relations in west Shetland. University of Liverpool PhD thesis.

Scherer, E., Münker, C. & Mezger, K. 2001 Calibration of the Lutetium–Hafnium Clock. *Science* **293**, 683-687.

Stern, R. 2001. A New Isotopic and Trace-Element Standard for the Ion-microprobe: Preliminary thermal Ionisation Mass Spectrometry (TIMS) U–Pb and Electron Microprobe Data. Geological Survey of Canada, Radiogenic Age and Isotope Studies, Report 14, Current Research 2001-F1. 11pp.

Stern, R.A., Bodorkos, S., Kamo, S.L., Hickman, A.H. & Corfu, F. 2009. Measurement of SIMS instrumental mass fractionation of Pb isotopes during zircon dating. *Geostandards and Geoanalytical Research,* **33**, 145-168.

St-Onge, M., van Gool, J.A.M., Garde, A.A. & Scott, D. 2009. Correlation of Archaean and Palaeoproterozoic units between northeastern Canada and western Greenland: constraining the pre-collisional upper plate history of the Trans-Hudson orogen. *In*: Cawood, P.A. & Kroner, A. (eds), *Earth Accretionary Orogens in Time and Space*. Geological Society, London, Special Publications, **318**, 193-235.

Sun, S.S. & McDonough, W.F. 1989. Chemical and isotopic systematics of oceanic basalts; implications for mantle composition and processes. *In:* Saunders, A.D. & Norry, M.J. (Eds), *Magmatism in the ocean basins.* Geological Society, London, Special Publications, 42, 313-345.

Walker, S., Thirlwall, M.F., Strachan, R.A. & Bird, A.F. 2016. Evidence from Rb–Sr mineral ages for multiple orogenic events in Caledonides of the Shetland Islands, Scotland. *Journal of the Geological Society, London,* **173**, 489-503.

Wheeler, J., Park, R.G., Rollinson, H.R. & Beach, A. 2010. The Lewisian Complex: insights into deep crustal evolution. *In*: Law, R.D., Butler, R.W.H., Holdsworth, R.E., Krabbendam, M. & Strachan, R.A. (eds). *Continental Tectonics and Mountain Building: The Legacy of Peach and Horne*. Geological Society, London, Special Publications, **335**, 51-79.

Whitehouse, M.J. 1993. Age of the Corodale gneisses, South Uist. *Scottish Journal of Geology*, **29**, 1-7.

Whitehouse, M.J. & Bridgwater, D. 2001. Geochronological constraints on Palaeoproterozoic crustal evolution and regional correlations of the northern Outer Hebridean Lewisian complex. *Precambrian Research*, **105**, 227-245.

Whitehouse, M.J. & Kemp, A.J.S. 2010. On the difficulty of assigning crustal residence, magmatic protolith and metamorphic ages to Lewisian granulites: constraints from combined *in situ* U–Pb and Lu–Hf isotopes. *In*: Law, R.D., Butler, R.W.H., Holdsworth, R.E.,

Krabbendam, M. & Strachan, R.A. (eds). *Continental Tectonics and Mountain Building: The Legacy of Peach and Horne*. Geological Society, London, Special Publications, **335**, 81-101.

Whitehouse, M.J., Fowler, M.B. & Friend, C.R.L. 1996. Conflicting mineral and whole-rock isochron ages from the Late-Archaean Lewisian Complex of northwestern Scotland: Implications for geochronology in polymetamorphic high-grade terrains. *Geochimica et Cosmochimica Acta*, **60,** 3085-3102.

Figure captions

Fig 1. (a) Location of Shetland with respect to the main British Isles. Abbreviations: HF, Hebridean Foreland; MT, Moine Thrust; WKSZ, Wester Keolka Shear Zone; GGF, Great Glen Fault; WBF, Walls Boundary Fault; HBF, Highland Boundary Fault; SUF, Southern Uplands Fault; IS, Iapetus Suture. (b) Geology of the northern half of Shetland, showing the location of the study area (Fig. 2). U, Uyea; USZ, Uyea Shear Zone; RV, Ronas Voe; F, Fethaland; CI, Cullivoe Inlier. Other abbreviations as for map (a).

Fig 2. (a) Detailed lithological map of the coastline at Uyea, showing structural data and dated sample localities. USZ, Uyea Shear Zone. (b) and (c) Stereonet compilations of foliation orientations west and east of the Uyea Shear Zone, respectively.

Fig 3. Photographs of various components of the Uyea Gneiss Complex. A) Augen facies of the granitic gneiss, close to S05-11 sample site; B) Fugla Ness metagabbro close to S05-10 sample site, note relict sub-ophitic texture; C) coarse-grained hornblendite within the Fugla Ness metagabbro; D) intermingled coarse- and fine-grained facies of the metagabbro; E) weakly deformed metagabbro (MG) cutting discordantly across tightly folded granitic gneiss; F) folded blastomylonitic fabric of granitc gneiss above the Uyea Shear Zone.

Fig 4. Summary geochemistry of Uyea orthogneisses: A) TAS diagram, B) AFM diagram, C) Chondrite-normalized REE plots, D) Primitive mantle-normalized plots. Normalizing values from Sun and McDonough, 1989. Stars = hornblendites, open diamonds = metagabbros, closed diamonds = granitic gneisses, open crosses = mafic enclaves in granitic gneisses.

Fig 5. Cathodoluminescence (CL) images of selected, representative zircons from the Uyea Gneiss Complex. A) Zircons from granitic gneiss samples; B) Zircons from metagabbro

samples. Ages of marked spots are $^{207}Pb/^{206}Pb$ ages in Ma ± 1σ uncertainty. Images were obtained using a Phillips XL30 scanning electron microscope at the John de Laeter Centre, Perth, using a 12kV electron beam and monochromatic CL detector.

Fig 6. Concordia plots of SHRIMP zircon U–Pb data for the Uyea Gneiss Complex. Ellipses show 1σ uncertainties of individual spot analyses. A) Zircons from granitic gneiss samples; B) Zircons from metagabbro samples. Data from Table 2. Analyses shaded red denote magmatic zircon; blue denotes zircon rims and/or recrystallized areas; green denotes older cores; grey denotes analyses more than 5% discordant. Ages labelled on Concordia are Ma.

Fig 7. Hafnium isotope evolution diagram. Individual analyses of the North Roe zircons are shown as red dots (granitic gneisses - magmatic), blue dots (granitic gneisses – zircon cores) and green dots (metagabbro zircons). Fields for the Gruinard and Assynt Terranes of the Lewisian Gneiss Complex are based on Hf data of Love (2003) for c. 2825 Ma tonalite samples GL00/06 and GL00/09, and c. 2900 Ma trondhjemite sample S98/1 (Love et al. 2004, 2010). Two Assynt Terrane tonalite samples studied by Whitehouse and Kemp (2010) have similar ranges in zircon Hf compositions to S98/1, but their interpreted protolith ages differ. The shaded field shows the overall range in Lewisian TTG-suite orthogneiss protolith ages from all sub-terranes and inliers (Kinny & Friend, 1997, Friend & Kinny 2001, Kinny et al. 2005, Friend et al. 2008, Love et al. 2010). The field labelled metamorphism refers specifically to the time of zircon rim growth/recrystallization in the Gruinard Terrane (Love et al. 2004).

Fig 8. Simplified map reconstruction showing the major age provinces within the British Isles, Ireland and Greenland, the ages of the most recent significant orogenic activity in each, and the zircon U–Pb ages obtained from basement rocks sampled in boreholes north and west of Shetland (Chambers et al. 2005, Holdsworth et al. 2019). Abbreviations: MT, Moine Thrust; IS, Iapetus Suture; MP, Midland Platform; NR, North Roe; VF, Variscan Front. RC and AGC denote the Rhinns Complex and Annagh Gneiss Complex, respectively, both of which represent extensions of the Ketilidean Province.

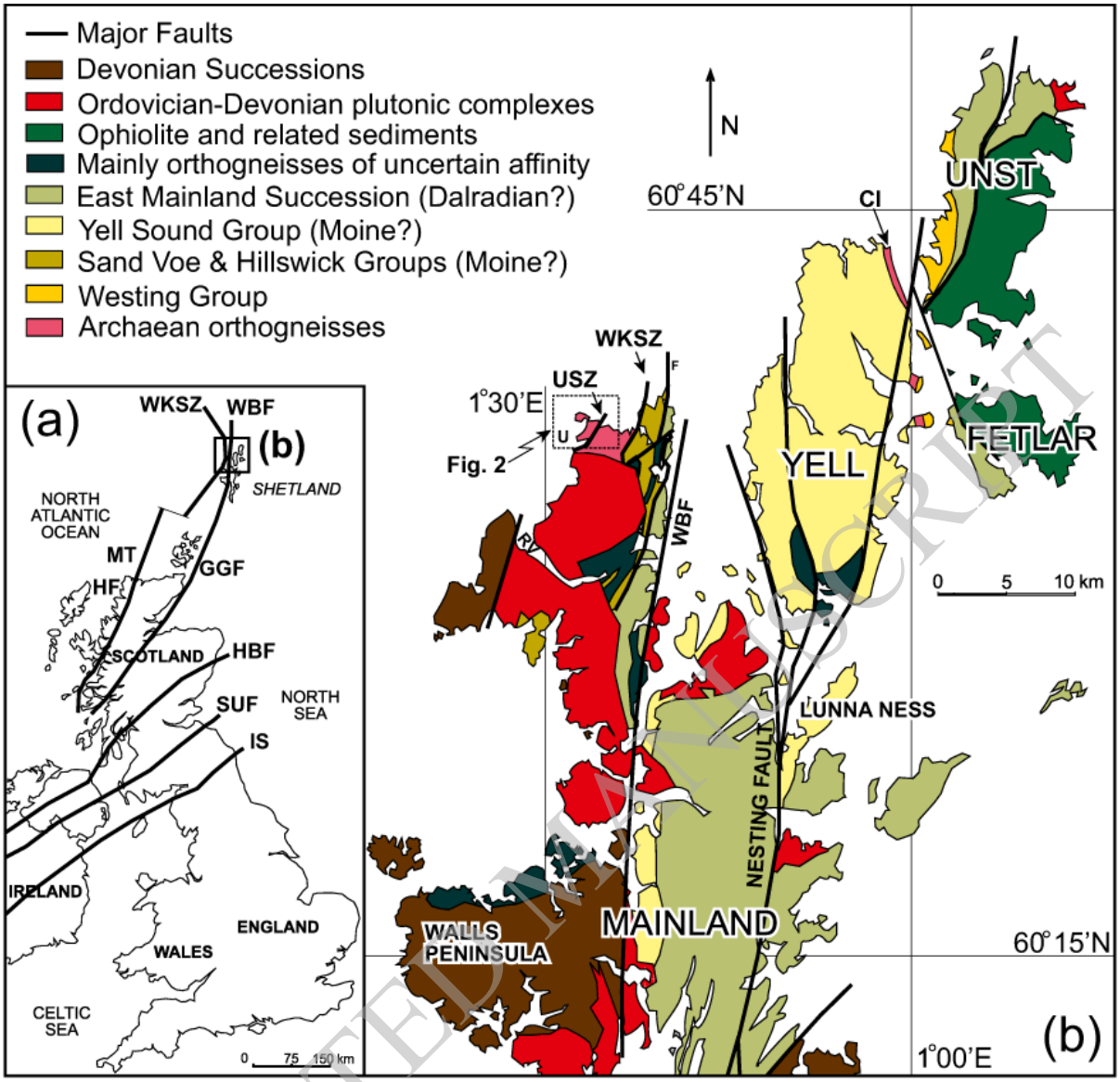

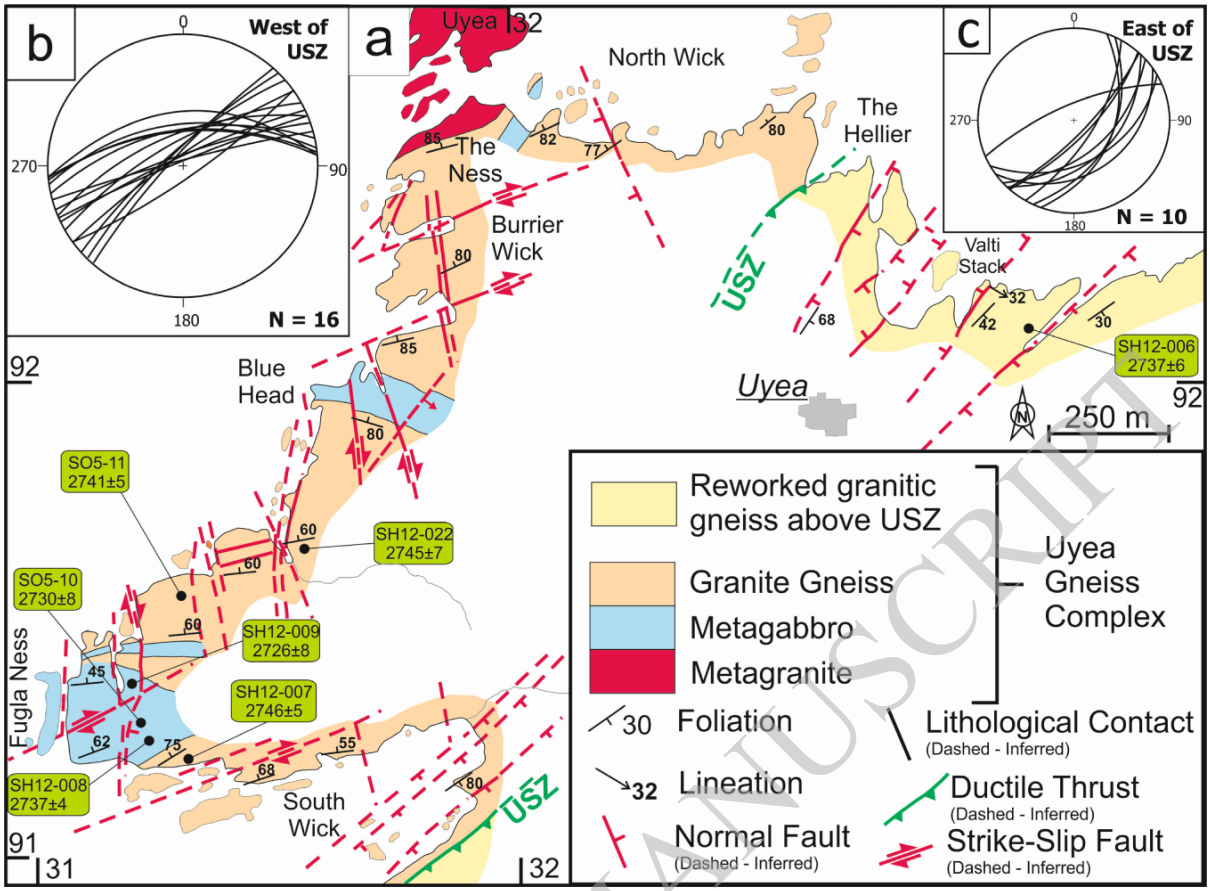

Fig.4

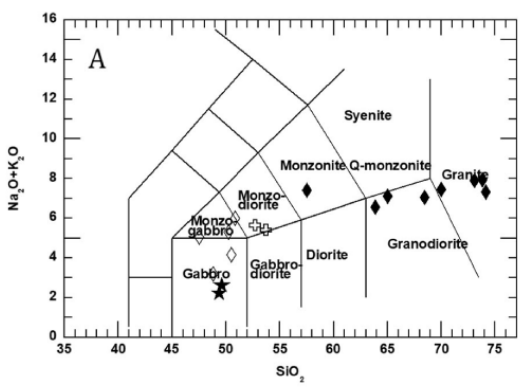

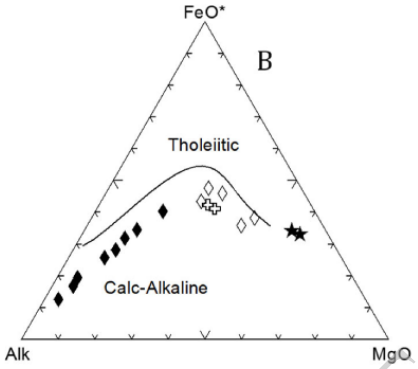

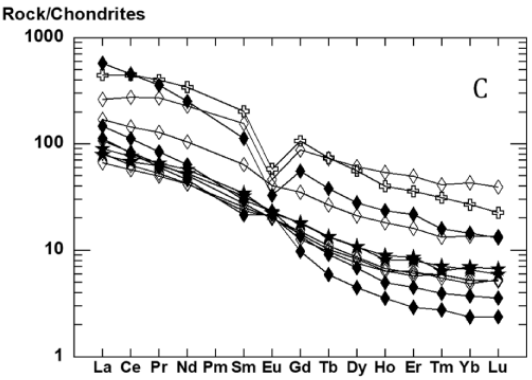

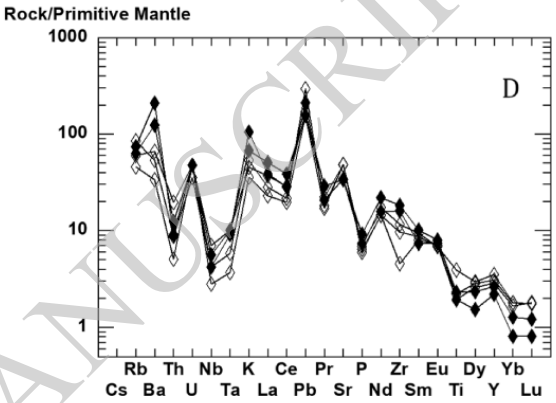

Fig.5

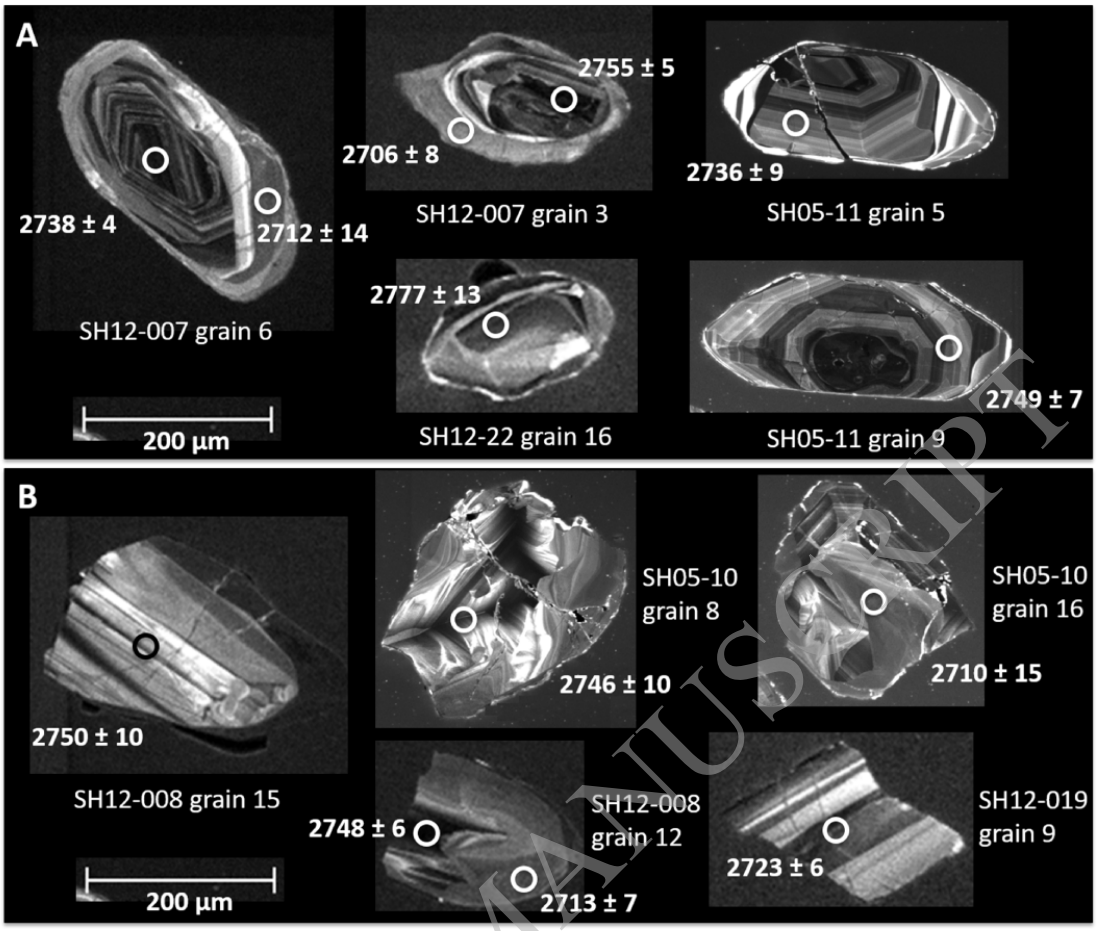

Fig.6

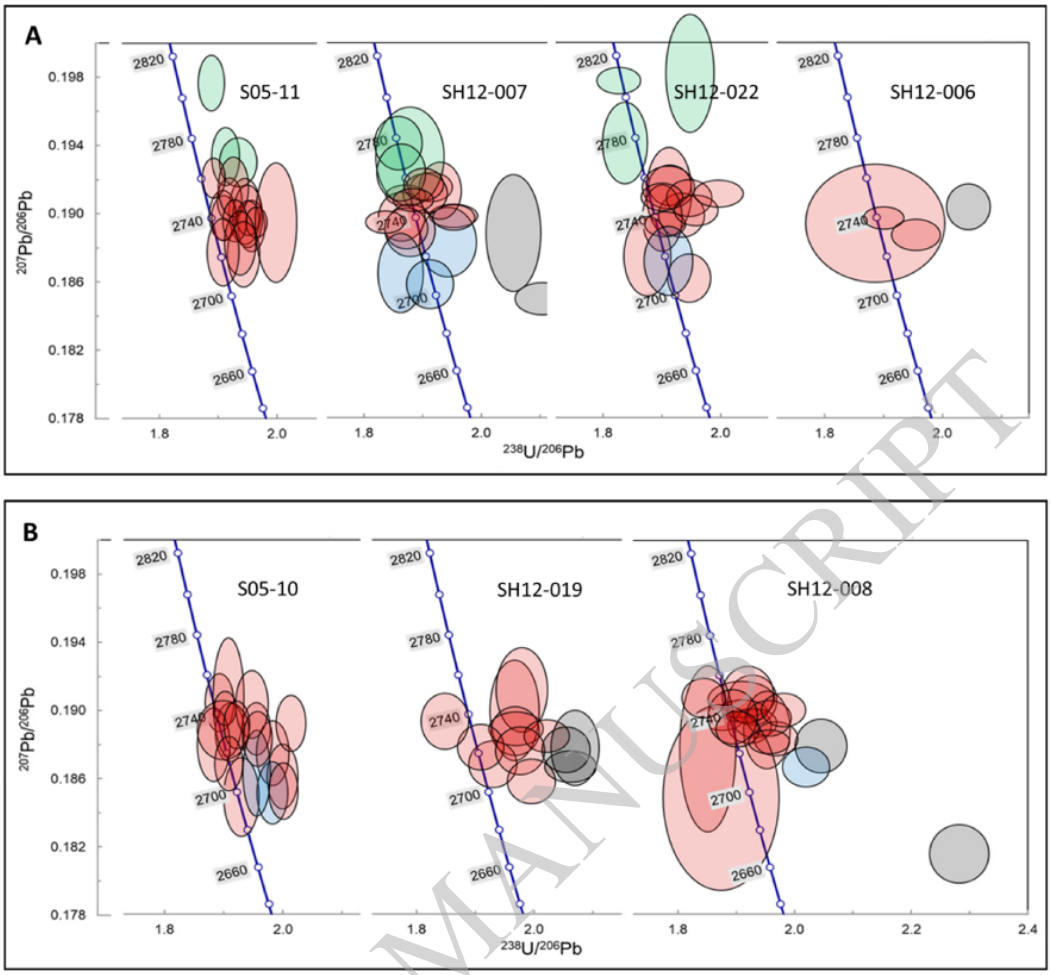

Fig.7

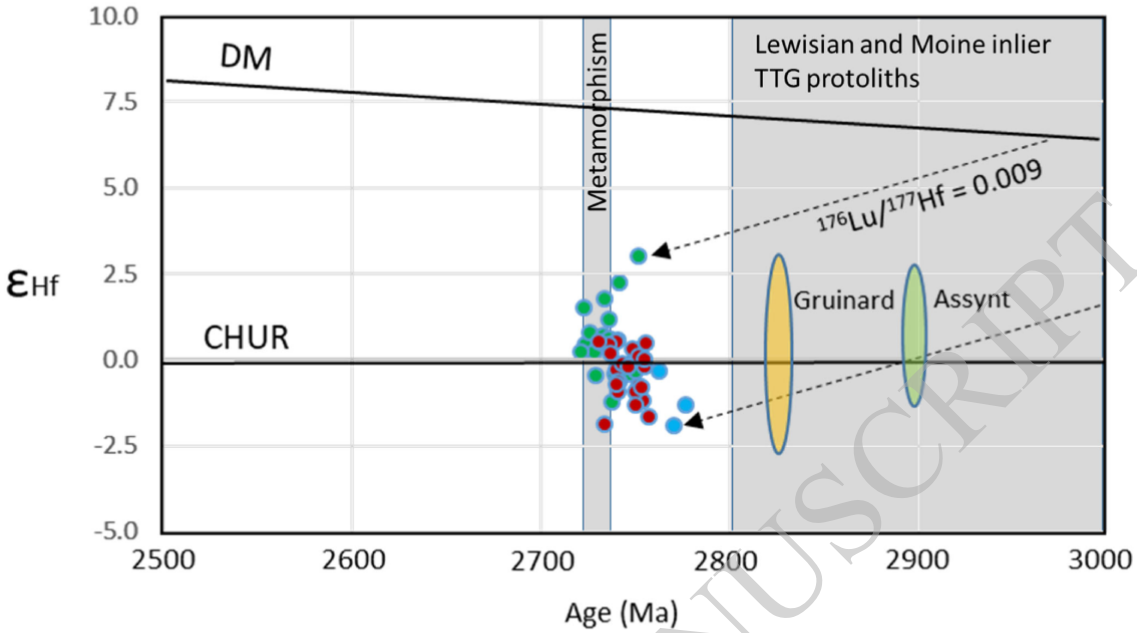

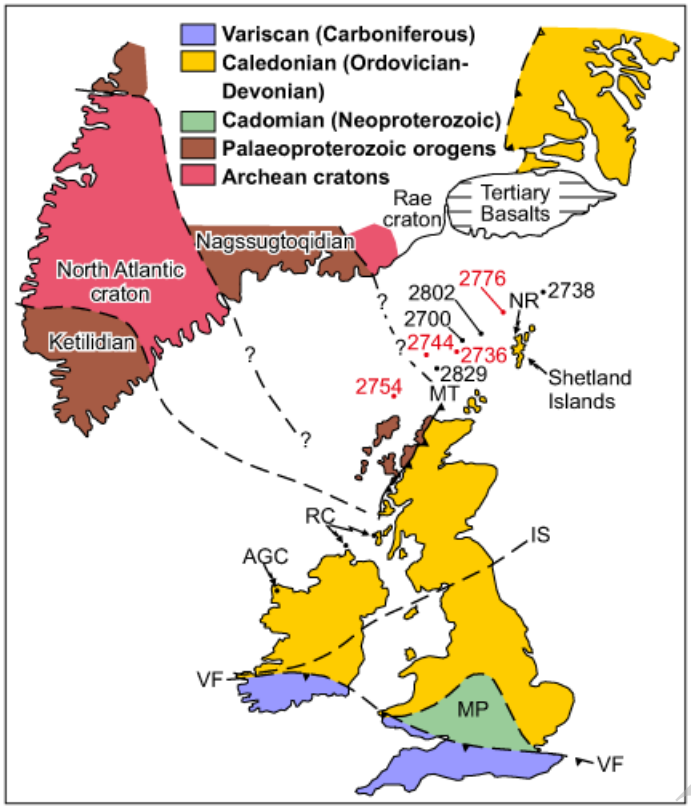

Table 1. Representative major and trace element data for the Uyea metagabbro and granitic gneisses from North Roe, Shetland

Columns 1 to 6 (11FG03 – 11FG06) are samples of metagabbro. Columns 7 to 9 (08NR05 – 11FG05) are samples of granitic gneiss. L.O.I. = loss on ignition; bdl = below detection limit.

	11FG03	08NR01	08NR04	08NR02	08NR07	11FG06	08NR05	11FG04	11FG05
SiO_2	48.24	46.80	48.32	49.98	50.50	51.74	56.49	66.95	68.88
TiO_2	0.59	1.89	0.42	1.13	1.01	1.83	0.98	0.50	0.42
Al_2O_3	10.07	17.77	18.49	18.27	13.90	17.57	17.10	15.73	15.35
Fe_2O_3	10.66	11.53	7.42	9.84	13.18	9.06	8.01	3.65	3.29
MnO	0.16	0.10	0.18	0.14	0.20	0.15	0.10	0.04	0.05
MgO	15.89	7.19	7.85	5.57	7.81	5.72	3.30	1.36	1.13
CaO	9.89	9.05	9.43	7.86	10.79	4.85	5.12	2.68	1.99
Na_2O	1.55	3.35	2.54	4.48	2.03	5.32	4.83	5.01	4.28
K_2O	1.06	1.69	1.61	1.51	0.38	0.08	2.57	2.03	3.16
P_2O_5	0.18	0.24	0.13	0.46	0.09	0.92	0.48	0.20	0.16
L.O.I.	1.24	1.08	3.18	1.25	1.01	2.41	1.68	2.05	1.89
Total	99.53	100.69	99.57	100.49	100.90	99.65	100.66	100.20	100.60
Sc	33	40	29	51	45	33	24	bdl	bdl
Cr	741	8	13	4	105	22	17	19	21
V	191	468	168	263	308	118	125	50	49
Cu	16	98	115	109	70	65	35	36	11
Zn	90	77	69	140	109	142	112	48	50
Ni	575	57	89	25	59	30	21	bdl	bdl
Rb	25	48	54	35	8	2	56	40	47
Sr	338	878	1016	744	206	715	692	709	720
Y	17	33	13	96	25	56	44	12	10
Zr	73	117	51	54	61	267	286	204	179
Nb	3	10	3	22	2	25	9	4	3
Ba	196	687	373	524	100	61	617	867	1467

Pb	37	4	21	12	6	16	6	11	15
U	1.0	1.8	0.7	0.6	0.2	bdl	0.6	1.0	1.0
Th	3.7	2.5	0.7	1.1	0.5	2.8	13.7	1.1	0.8
Hf	2.7	2.8	0.9	1.7	1.3	8.4	7.0	6.4	4.5
Ta	0.3	1.3	0.2	1.9	0.6	0.8	1.2	0.4	0.4
La	21.3	40.1	19.3	62.1	6.85	105	136	34.7	26.5
Ce	46.4	87.9	38.3	168	13.3	272	278	68.4	50.1
Pr	6.22	12.2	4.99	25.8	1.92	37.9	33.9	7.97	5.70
Nd	26.7	48.6	19.6	106	8.22	160	117	29.6	21.3
Sm	5.22	9.72	3.55	23.7	2.37	30.9	17.2	4.50	3.27
Eu	1.29	2.33	1.20	2.67	0.87	3.35	1.89	1.34	1.25
Gd	3.72	7.16	2.60	17.9	2.61	21.9	11.3	2.78	2.00
Tb	0.50	0.99	0.36	2.71	0.49	2.75	1.41	0.34	0.22
Dy	2.75	5.33	1.91	15.4	3.20	14.1	7.04	1.73	1.13
Ho	0.46	1.02	0.36	3.03	0.75	2.25	1.32	0.28	0.20
Er	1.32	2.65	1.05	8.17	2.02	5.90	3.57	0.74	0.48
Tm	0.18	0.34	0.14	1.05	0.27	0.79	0.40	0.10	0.07
Yb	1.11	2.30	0.82	7.27	1.93	4.55	2.44	0.63	0.40
Lu	0.15	0.34	0.13	0.99	0.28	0.57	0.33	0.09	0.06

Table 2. SHRIMP U-Pb age data for samples from North Roe, Shetland

Data corrected for common Pb using the measured ^{204}Pb. %common ^{206}Pb is defined as $(^{204}Pb/^{206}Pb)_{measured}/(^{204}Pb/^{206}Pb)_{common}$ x100. High ^{204}Pb analyses excluded. Pb* refers to radiogenic Pb. %Discordance is defined as (1 – ($^{206}Pb/^{238}U$ Age)/($^{207}Pb/^{206}Pb$ Age)) x100.

Grain-Spot	Location	U ppm	Th ppm	$\frac{^{232}Th}{^{238}U}$	%common ^{206}Pb	$\frac{^{238}U}{^{206}Pb^*}$	± 1σ	$\frac{^{207}Pb^*}{^{206}Pb^*}$	± 1σ	$^{206}Pb/^{238}U$ Age (Ma)	± 1σ	$^{207}Pb/^{206}Pb$ Age (Ma)	± 1σ	%Disc.
Sample S05-11 granitic gneiss *[HU 31320 91519]*														
1.1	outer	155	85	0.57	-0.01	1.943	0.018	0.1876	0.0013	2677	20	2722	11	2
2.1	outer	152	71	0.48	0.06	1.937	0.018	0.1883	0.0012	2683	20	2727	11	2
3.2	core	283	74	0.27	0.43	1.888	0.014	0.1977	0.0011	2740	17	2807	9	2
4.1	centre	261	416	1.65	0.04	1.934	0.021	0.1930	0.0009	2687	24	2768	8	3
5.2	centre	291	56	0.20	0.16	1.956	0.015	0.1893	0.0010	2662	17	2736	9	3
6.1	outer	164	73	0.46	0.08	1.945	0.018	0.1902	0.0013	2674	20	2743	11	3
7.1	centre	150	69	0.48	0.10	1.908	0.018	0.1878	0.0013	2717	21	2723	11	0
8.1	centre	409	229	0.58	0.01	1.892	0.013	0.1921	0.0008	2735	15	2760	7	1
9.1	centre	353	84	0.25	0.04	1.919	0.014	0.1908	0.0008	2704	16	2749	7	2
10.1	centre	328	90	0.28	0.02	1.910	0.014	0.1898	0.0009	2715	16	2740	8	1
11.1	centre	203	74	0.38	0.06	1.998	0.023	0.1895	0.0023	2616	25	2738	20	4
12.1	centre	259	49	0.20	0.07	1.908	0.015	0.1899	0.0010	2717	17	2742	8	1
13.1	centre	188	71	0.39	0.25	1.950	0.017	0.1899	0.0012	2669	19	2741	10	3
14.1	uniform core	206	105	0.53	0.04	1.912	0.016	0.1934	0.0011	2712	18	2771	10	2
15.1	centre	182	76	0.43	0.01	1.926	0.017	0.1916	0.0012	2696	19	2756	10	2
16.1	centre	565	124	0.23	0.04	1.950	0.013	0.1898	0.0007	2668	14	2740	6	3
17.1	centre	365	153	0.43	0.07	1.928	0.014	0.1896	0.0008	2693	15	2739	7	2
18.1	centre	704	144	0.21	-0.01	1.965	0.012	0.1895	0.0006	2652	13	2738	5	3
Sample SH12-007 granitic gneiss *[HU 31267 91206]*														
1.1	centre	256	123	0.50	0.34	1.871	0.024	0.1891	0.0008	2760	29	2734	7	-1
2.1	centre	954	608	0.66	0.01	1.901	0.022	0.1917	0.0006	2725	26	2757	5	1
3.1	centre	430	276	0.66	0.04	1.915	0.024	0.1915	0.0006	2709	27	2755	5	2

3.2	uniform rim	157	93	0.61	-0.10	1.912	0.027	0.1858	0.0009	2712	31	2706	8	0
4.1	centre	817	882	1.12	0.06	1.953	0.023	0.1898	0.0005	2665	26	2740	4	3
5.1	centre	685	706	1.07	0.09	1.952	0.027	0.1898	0.0005	2666	30	2741	4	3
5.2	outer	117	84	0.74	0.85	2.054	0.031	0.1888	0.0023	2557	32	2732	20	6
6.1	centre	795	708	0.92	0.02	1.836	0.022	0.1895	0.0004	2803	27	2738	4	-2
6.2	uniform rim	157	97	0.64	0.43	1.862	0.025	0.1865	0.0015	2771	31	2712	14	-2

Table 2 ...

Grain-Spot	Location	U ppm	Th ppm	$^{232}Th/^{238}U$	%common ^{206}Pb	$^{238}U/^{206}Pb^*$	± 1σ	$^{207}Pb^*/^{206}Pb^*$	± 1σ	$^{206}Pb/^{238}U$ Age (Ma)	± 1σ	$^{207}Pb/^{206}Pb$ Age (Ma)	± 1σ	%Disc.
Sample SH12-007 granitic gneiss														
7.1	uniform core	35	38	1.12	0.05	1.878	0.038	0.1933	0.0019	2752	46	2771	16	1
8.1	centre	794	833	1.08	0.07	1.871	0.022	0.1911	0.0004	2760	27	2751	3	0
9.1	centre	276	125	0.47	0.07	1.904	0.025	0.1912	0.0008	2721	29	2752	7	1
10.1	centre	510	378	0.77	0.06	1.864	0.026	0.1898	0.0009	2768	31	2741	8	-1
11.1	core	486	216	0.46	0.14	2.103	0.030	0.1850	0.0006	2507	30	2698	5	7
11.2	outer	109	93	0.89	0.03	1.878	0.028	0.1890	0.0010	2751	33	2733	9	-1
12.1	sector core	135	172	1.32	-0.07	1.858	0.027	0.1941	0.0010	2776	32	2777	9	0
13.1	centre	739	836	1.17	0.06	1.884	0.022	0.1908	0.0004	2745	27	2749	4	0
14.1	centre	423	307	0.75	0.17	1.930	0.024	0.1913	0.0011	2692	27	2754	9	2
14.2	uniform rim	296	198	0.69	3.31	1.943	0.032	0.1883	0.0013	2677	36	2727	12	2
15.1	centre	855	685	0.83	3.32	2.172	0.030	0.1841	0.0020	2441	28	2690	18	9
16.1	core	123	93	0.78	0.25	1.863	0.027	0.1924	0.0011	2770	33	2763	9	0
Sample SH12-022 granitic gneiss *[HU 31592 91753]*														
1.1	centre	501	477	0.98	0.09	1.900	0.023	0.1910	0.0005	2726	27	2750	5	1
1.2	uniform rim	103	68	0.68	0.67	1.911	0.027	0.1872	0.0013	2713	32	2718	12	0
2.1	centre	241	139	0.60	-0.03	1.946	0.025	0.1909	0.0007	2673	29	2750	6	3
3.1	centre	550	210	0.39	2.45	1.946	0.024	0.1862	0.0009	2673	27	2709	8	1
4.1	centre	195	206	1.09	5.74	1.948	0.027	0.1982	0.0023	2671	30	2811	19	5

6.1	core	639	903	1.46	0.18	2.229	0.027	0.1849	0.0005	2389	24	2697	4	11
7.1	centre	253	142	0.58	1.39	1.912	0.025	0.1913	0.0017	2712	29	2753	15	1
8.1	centre	389	301	0.80	0.04	1.958	0.024	0.1902	0.0006	2660	27	2743	5	3
9.1	centre	517	308	0.62	0.02	1.996	0.028	0.1911	0.0005	2618	30	2752	5	5
9.2	outer	186	77	0.43	0.03	1.933	0.026	0.1899	0.0009	2688	30	2741	7	2
10.1	centre	365	254	0.72	0.18	1.913	0.024	0.1916	0.0008	2710	28	2756	7	2
11.1	centre	149	170	1.18	0.04	1.875	0.026	0.1875	0.0015	2755	32	2720	14	-1
12.1	centre	582	539	0.96	2.35	1.911	0.029	0.1915	0.0008	2713	34	2755	7	2
13.1	centre	685	140	0.21	0.42	1.827	0.025	0.1978	0.0005	2814	31	2808	4	0
14.1	centre	840	953	1.17	2.30	1.900	0.022	0.1897	0.0013	2726	26	2740	11	1
16.1	uniform core	149	98	0.68	0.05	1.837	0.025	0.1941	0.0016	2802	31	2777	13	-1
17.1	centre	538	518	0.99	0.04	1.905	0.023	0.1893	0.0005	2720	27	2736	4	1

Table 2 …

Grain-Spot	Location	U ppm	Th ppm	$^{232}Th/^{238}U$	%common ^{206}Pb	$^{238}U/^{206}Pb^*$	± 1σ	$^{207}Pb^*/^{206}Pb^*$	± 1σ	$^{206}Pb/^{238}U$ Age ± 1σ (Ma)		$^{207}Pb/^{206}Pb$ Age (Ma)	± 1σ	%Disc.
Sample S05-10 meta-gabbro *[HU 31202 91237]*														
1.1	centre	217	90	0.43	0.06	2.005	0.016	0.1853	0.0011	2609	18	2700	10	3
2.1	sector	135	117	0.89	0.18	1.887	0.018	0.1880	0.0014	2742	22	2725	13	-1
3.1	zoned	531	724	1.41	0.03	1.906	0.012	0.1901	0.0007	2719	14	2743	6	1
4.1	zoned	150	83	0.57	0.09	1.951	0.018	0.1903	0.0013	2667	20	2745	11	3
5.1	sector	219	128	0.60	0.04	2.017	0.016	0.1892	0.0011	2595	17	2735	9	5
6.1	zoned	300	363	1.25	0.06	1.926	0.014	0.1891	0.0009	2696	16	2735	8	1
7.1	centre	192	131	0.71	0.07	1.914	0.016	0.1887	0.0011	2709	19	2731	10	1
8.1	irregular	189	219	1.20	-0.02	1.896	0.016	0.1904	0.0011	2730	19	2746	10	1
9.1	centre	202	146	0.75	0.24	1.912	0.017	0.1908	0.0023	2712	20	2749	20	1
10.1	centre	209	166	0.82	0.03	1.961	0.016	0.1883	0.0011	2657	18	2728	9	3
11.1	zoned	157	118	0.77	-0.01	1.986	0.018	0.1875	0.0013	2629	20	2720	11	3
12.1	zoned	243	276	1.18	0.07	1.959	0.016	0.1889	0.0010	2659	17	2733	9	3
13.1	centre	204	51	0.26	0.46	2.003	0.017	0.1861	0.0013	2611	18	2708	11	4

14.1	centre	117	55	0.49	0.10	1.934	0.020	0.1849	0.0015	2687	23	2697	14	0
15.1	zoned	233	255	1.13	0.04	1.912	0.016	0.1869	0.0011	2712	18	2715	9	0
16.1	recrystallized	257	106	0.42	0.05	1.959	0.015	0.1863	0.0017	2659	17	2710	15	2
17.1	recrystallized	199	127	0.66	0.10	1.986	0.017	0.1851	0.0012	2629	19	2699	11	3
18.1	zoned	205	89	0.45	0.05	1.903	0.029	0.1888	0.0011	2723	34	2732	10	0
Sample SH12-008 meta-gabbro *[HU 31199 91232]*														
1.1	centre	130	71	0.57	0.10	1.894	0.028	0.1896	0.0011	2733	33	2739	9	0
2.1	centre	572	947	1.71	0.02	1.851	0.032	0.1877	0.0032	2785	39	2722	28	-2
3.1	centre crack	217	75	0.36	0.33	2.671	0.072	0.1828	0.0011	2050	47	2678	10	23
4.1	centre	161	61	0.39	0.16	2.045	0.029	0.1879	0.0010	2566	30	2724	9	6
4.2	outer	244	205	0.87	-0.00	1.902	0.025	0.1889	0.0007	2724	29	2733	6	0
5.1	centre	688	909	1.36	0.05	1.956	0.023	0.1882	0.0005	2662	26	2726	4	2
6.1	centre	208	228	1.13	0.15	1.947	0.026	0.1890	0.0015	2672	29	2733	13	2
7.1	centre	299	576	1.99	0.25	1.844	0.024	0.1907	0.0008	2793	30	2748	7	-2
7.2	outer	296	89	0.31	-0.03	1.923	0.024	0.1891	0.0007	2699	28	2734	6	1
8.1	centre	427	701	1.69	0.04	1.968	0.025	0.1883	0.0007	2649	27	2728	6	3
9.1	centre	904	2112	2.41	0.01	1.876	0.022	0.1895	0.0004	2754	27	2737	4	-1

Table 2 …

Grain-Spot	Location	U ppm	Th ppm	$^{232}Th/^{238}U$	%common ^{206}Pb	$^{238}U/^{206}Pb^*$	± 1σ	$^{207}Pb^*/^{206}Pb^*$	± 1σ	$^{206}Pb/^{238}U$ Age ± 1σ (Ma)		$^{207}Pb/^{206}Pb$ Age ± 1σ (Ma)		%Disc.
10.1	sector	187	60	0.33	0.03	1.928	0.028	0.1906	0.0010	2694	32	2747	8	2
11.1	zoned	555	965	1.80	0.00	1.933	0.024	0.1893	0.0006	2688	27	2736	5	2
12.1	centre	344	525	1.58	-0.01	1.908	0.038	0.1907	0.0007	2716	44	2748	6	1
12.2	outer	213	63	0.30	-0.04	2.019	0.027	0.1867	0.0008	2593	28	2713	7	4
13.1	sector	433	588	1.40	0.05	1.981	0.025	0.1900	0.0007	2634	27	2742	6	4
15.1	centre	153	60	0.41	-0.03	1.919	0.029	0.1909	0.0011	2703	33	2750	10	2
16.1	sector	408	352	0.89	0.05	1.955	0.025	0.1896	0.0007	2663	28	2738	6	3
16.2	dark sector	356	119	0.34	1.13	1.874	0.066	0.1849	0.0036	2757	78	2697	32	-2

17.1	irregular	174	88	0.52	0.15	2.281	0.034	0.1815	0.0011	2343	29	2667	10	12
18.1	centre	944	1876	2.05	0.00	1.911	0.027	0.1900	0.0004	2713	31	2742	4	1
Sample SH12-019 meta-gabbro *[HU 31215 91356]*														
1.2	sector	201	91	0.47	0.23	2.054	0.027	0.1877	0.0009	2557	28	2722	8	6
2.1	centre	307	131	0.44	0.06	1.969	0.030	0.1889	0.0006	2648	33	2733	6	3
3.1	core	166	129	0.80	1.00	1.967	0.027	0.1900	0.0020	2650	30	2742	17	3
4.2	sector	155	112	0.75	0.09	1.930	0.027	0.1868	0.0009	2692	31	2714	8	1
5.1	centre	123	82	0.69	0.63	1.979	0.029	0.1912	0.0016	2637	32	2752	14	4
6.1	centre	342	281	0.85	0.05	2.021	0.025	0.1885	0.0006	2591	27	2729	6	5
7.1	centre	254	258	1.05	0.23	2.070	0.027	0.1878	0.0015	2541	27	2723	13	7
8.1	centre	182	193	1.10	0.12	1.968	0.027	0.1888	0.0009	2649	30	2732	8	3
9.1	centre	176	202	1.19	0.07	1.909	0.026	0.1878	0.0009	2716	30	2723	8	0
10.1	centre	163	117	0.74	-0.05	1.976	0.028	0.1876	0.0009	2640	30	2721	8	3
11.1	centre	329	372	1.17	0.15	1.848	0.027	0.1893	0.0011	2788	33	2736	9	-2
12.1	core	154	111	0.75	0.10	1.995	0.027	0.1858	0.0009	2619	29	2705	8	3
13.1	core	331	284	0.88	0.05	2.062	0.029	0.1867	0.0006	2549	29	2713	5	6
Sample SH12-006 granitic gneiss *[HU 33077 92135]*														
1.1	centre	607	490	0.83	0.02	1.900	0.023	0.1897	0.0004	2726	27	2740	4	1
3.1	centre	440	324	0.76	0.15	1.886	0.078	0.1894	0.0023	2743	92	2737	20	0
4.1	centre	592	497	0.87	0.56	2.044	0.025	0.1904	0.0009	2568	25	2746	8	6
5.1	outer	136	85	0.64	0.16	2.266	0.033	0.1849	0.0011	2357	29	2697	9	13
6.1	centre	355	205	0.60	0.05	1.955	0.027	0.1887	0.0006	2664	30	2731	5	2

Table 3. LA-ICP-MS Hafnium isotope data for zircons from North Roe, Shetland

Age (Ma) is the $^{207}Pb/^{206}Pb$ age from Table 2. ^{176}Lu decay constant 1.865 x 10^{-11} y^{-1} (Scherer et al. 2001). CHUR parameters, used to calculate εHf values, are after Blichert-Toft & Albarède (1997). Depleted mantle (DM) parameters after Griffin et al. (2000). Single stage T_{DM} model age uses the measured zircon $^{176}Lu/^{177}Hf$ ratio; two stage T_{DM} model age assumes that the precursor crust had $^{176}Lu/^{177}Hf$ of 0.009 (Gardiner et al. 2018).

Grain-Spot	$^{176}Hf/^{177}Hf$	± 1σ	$^{176}Lu/^{177}Hf$	$^{176}Yb/^{177}Hf$	$^{176}Hf/^{177}Hf$ init.	Age (Ma)	εHf	± 1σ	T_{DM} (Ga)	T_{DM} (2 stage)
Sample SH12-007 granitic gneiss *[HU 31267 91206]*										
1.1	0.2810320	0.0000054	0.0009408	0.0337200	0.280983	2734	-1.87	0.19	3.08	3.21
2.1	0.2810500	0.0000110	0.0014361	0.0503342	0.280974	2757	-1.64	0.39	3.10	3.21
3.1	0.2810510	0.0000074	0.0006748	0.0249827	0.281015	2755	-0.22	0.26	3.04	3.14
4.1	0.2810650	0.0000066	0.0007908	0.0300044	0.281024	2740	-0.28	0.23	3.03	3.13
5.1	0.2810980	0.0000070	0.0017738	0.0734889	0.281005	2741	-0.92	0.25	3.06	3.16
7.1	0.2809830	0.0000083	0.0005009	0.0207005	0.280956	2771	-1.95	0.29	3.12	3.24
8.1	0.2810610	0.0000084	0.0012255	0.0482145	0.280996	2751	-0.99	0.29	3.07	3.17
9.1	0.2810420	0.0000053	0.0007647	0.0295651	0.281002	2752	-0.78	0.19	3.06	3.16
10.1	0.2810710	0.0000078	0.0011144	0.0416684	0.281013	2741	-0.65	0.27	3.05	3.15
12.1	0.2810230	0.0000090	0.0009933	0.0430561	0.280970	2777	-1.32	0.32	3.10	3.21
13.1	0.2811120	0.0000079	0.0014764	0.0547688	0.281034	2749	0.31	0.28	3.02	3.11
14.1	0.2810470	0.0000076	0.0011040	0.0383767	0.280989	2754	-1.19	0.27	3.08	3.19
16.1	0.2810520	0.0000066	0.0008645	0.0364302	0.281006	2763	-0.36	0.23	3.05	3.15
Sample SH12-022 granitic gneiss *[HU 31592 91753]*										
1.1	0.2810400	0.0000085	0.0007734	0.0305925	0.280999	2750	-0.91	0.30	3.06	3.17
2.1	0.2810200	0.0000075	0.0006042	0.0221628	0.280988	2750	-1.30	0.26	3.07	3.19
7.1	0.2810390	0.0000047	0.0007376	0.0288684	0.281000	2753	-0.81	0.16	3.06	3.17
8.1	0.2810730	0.0000067	0.0009031	0.0364373	0.281026	2743	-0.14	0.23	3.03	3.12
9.1	0.2810740	0.0000049	0.0009131	0.0355740	0.281026	2752	0.08	0.17	3.03	3.12
9.2	0.2811080	0.0000038	0.0011729	0.0491752	0.281046	2741	0.56	0.13	3.00	3.09
10.1	0.2810890	0.0000060	0.0010379	0.0419153	0.281034	2756	0.47	0.21	3.01	3.10

12.1	0.2811020	0.0000062	0.0015182	0.0600789	0.281022	2755	0.01	0.22	3.04	3.13
14.1	0.2810930	0.0000056	0.0008866	0.0333653	0.281047	2740	0.54	0.20	3.00	3.09

Table 3 …

Grain-Spot	$^{176}Hf/^{177}Hf$	± 1σ	$^{176}Lu/^{177}Hf$	$^{176}Yb/^{177}Hf$	$^{176}Hf/^{177}Hf$ init.	Age (Ma)	εHf	± 1σ	T_{DM} (Ga)	T_{DM} (2 stage)
Sample SH12-006 granitic gneiss *[HU 33077 92135]*										
1.1	0.2810550	0.0000078	0.0007318	0.0286162	0.281017	2740	-0.73	0.27	3.04	3.14
3.1	0.2810980	0.0000053	0.0011275	0.0432126	0.281039	2737	0.20	0.19	3.01	3.10
4.1	0.2810910	0.0000076	0.0013211	0.0513234	0.281022	2746	-0.21	0.27	3.03	3.13
6.1	0.2810910	0.0000068	0.0007461	0.0273747	0.281052	2731	0.53	0.24	2.99	3.08
Sample SH12-008 meta-gabbro *[HU 31199 91232]*										
1.1	0.2810480	0.0000060	0.0005248	0.0223051	0.281020	2739	-0.41	0.21	3.03	3.14
4.1	0.2810680	0.0000062	0.0002746	0.0106175	0.281054	2724	0.42	0.22	2.98	3.08
5.1	0.2811580	0.0000099	0.0018415	0.0899245	0.281062	2726	0.76	0.35	2.98	3.06
6.1	0.2810910	0.0000110	0.0007362	0.0287890	0.281053	2733	0.59	0.39	2.99	3.08
7.2	0.2811630	0.0000110	0.0014797	0.0606682	0.281086	2734	1.79	0.39	2.95	3.02
8.1	0.2810980	0.0000073	0.0010106	0.0457624	0.281045	2728	0.22	0.26	3.00	3.09
9.1	0.2811400	0.0000077	0.0017555	0.0834724	0.281048	2737	0.53	0.27	3.00	3.09
10.1	0.2810300	0.0000045	0.0002794	0.0109640	0.281015	2747	-0.41	0.16	3.04	3.14
11.1	0.2811550	0.0000110	0.0016928	0.0742546	0.281066	2736	1.15	0.39	2.98	3.05
12.1	0.2810480	0.0000033	0.0004799	0.0195828	0.281023	2748	-0.12	0.12	3.03	3.13
15.1	0.2810520	0.0000083	0.0006863	0.0296036	0.281016	2750	-0.32	0.29	3.04	3.14
16.1	0.2810610	0.0000067	0.0012041	0.0517668	0.280998	2738	-1.24	0.23	3.07	3.18
18.1	0.2811310	0.0000069	0.0022526	0.1066290	0.281013	2742	-0.61	0.24	3.05	3.15

Sample SH12-019 meta-gabbro *[HU 31215 91356]*

2.1	0.2810730	0.0000077	0.0003432	0.0119369	0.281055	2733	0.68	0.27	2.98	3.07
3.1	0.2811070	0.0000100	0.0002537	0.0094182	0.281094	2742	2.26	0.35	2.93	3.00
5.1	0.2811210	0.0000085	0.0002449	0.0079414	0.281108	2752	3.01	0.30	2.91	2.97
6.1	0.2810560	0.0000094	0.0005817	0.0210215	0.281026	2729	-0.46	0.33	3.02	3.13
8.1	0.2810780	0.0000088	0.0005318	0.0196299	0.281050	2732	0.49	0.31	2.99	3.08
9.1	0.2811050	0.0000084	0.0003928	0.0138406	0.281085	2723	1.50	0.29	2.94	3.02
10.1	0.2810700	0.0000067	0.0003700	0.0133525	0.281051	2721	0.25	0.23	2.99	3.09
11.1	0.2810910	0.0000086	0.0007544	0.0278040	0.281052	2736	0.62	0.30	2.99	3.08
